(19) Europäisches Patentamt
European Patent Office
Office européen des brevets

(11) EP 1 879 291 A1

(12) EUROPEAN PATENT APPLICATION

published in accordance with Art. 153(4) EPC

(43) Date of publication:
16.01.2008 Bulletin 2008/03

(21) Application number: **06713834.7**

(22) Date of filing: **16.02.2006**

(51) Int Cl.:
H03H 9/145 *(2006.01)* ***H01L 41/09*** *(2006.01)*
H01L 41/18 *(2006.01)* ***H01L 41/187*** *(2006.01)*
H03H 9/25 *(2006.01)*

(86) International application number:
PCT/JP2006/302693

(87) International publication number:
WO 2006/114930 (02.11.2006 Gazette 2006/44)

(84) Designated Contracting States:
AT BE BG CH CY CZ DE DK EE ES FI FR GB GR HU IE IS IT LI LT LU LV MC NL PL PT RO SE SI SK TR

(30) Priority: **25.04.2005 JP 2005126674**

(71) Applicant: **MURATA MANUFACTURING CO., LTD.**
Nagaokakyo-shi, Kyoto 617-8555 (JP)

(72) Inventor: **KANDO, Hajime,**
c/o MURATA MANUFACTURING CO., LTD.
Nagaokakyo-shi,
Kyoto 617-8555 (JP)

(74) Representative: **Stöckeler, Ferdinand et al**
Schoppe, Zimmermann,
Stöckeler & Zinkler
Postfach 246
82043 Pullach bei München (DE)

(54) BOUNDARY ACOUSTIC WAVE DEVICE

(57) To provide a boundary acoustic wave device that efficiently confines the vibrational energy of boundary acoustic waves and exhibits a high electromechanical coupling coefficient, and is consequently not affected by higher-order modes.

The boundary acoustic wave device includes a first medium 11 having piezoelectric characteristics, a non-electroconductive second medium 12, and a third medium 13 through which slow transverse waves propagate at a lower acoustic velocity than slow transverse waves propagating through the first and second media 11 and 12. The first medium 11, the third medium 13, and the second medium 12 are stacked in that order. An IDT 14 is disposed between the first medium 11 and the third medium 13. The IDT 14 includes a metal layer made of a metal having a density ρ in the range of 3000 to 21500 kg/m^3. The IDT 14 has electrode fingers at a pitch of λ and has a thickness H1 satisfying the relationship $0.006\lambda \leq H1 \leq 0.2\lambda$, and the third medium 13 has a thickness H2 satisfying the relationship $H1 < H2 \leq 0.7\lambda$.

FIG. 2

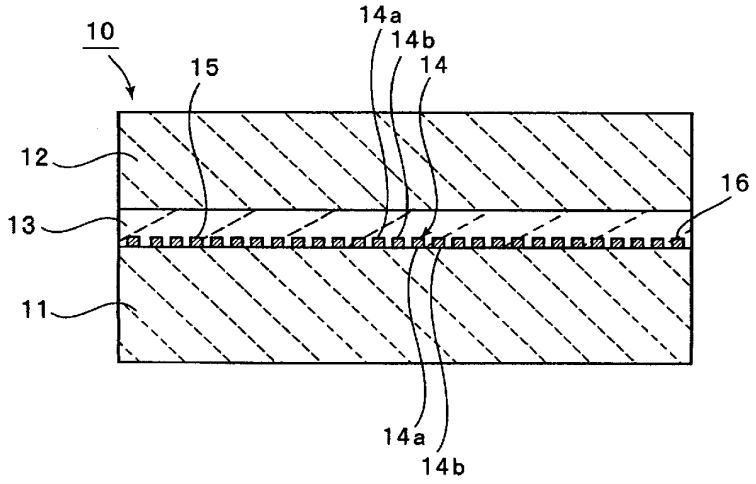

EP 1 879 291 A1

Description

Technical Field

[0001] The present invention relates to boundary acoustic wave devices using boundary acoustic waves propagating along the interface between different media, and more particularly to a boundary acoustic wave device including a multilayer structure formed by stacking at least three media.

Background Art

[0002] A variety of devices using boundary acoustic waves, such as resonators and band-pass filters, have been proposed. Boundary acoustic waves propagate along the interface between different media. Therefore the packages of boundary acoustic wave devices can be simpler than those of surface acoustic wave devices using surface acoustic waves. The boundary acoustic wave device thus can be more simplified, and its thickness can be reduced.

[0003] Non-Patent Document 1 has disclosed a boundary acoustic wave device. The boundary acoustic wave device has a multilayer structure including a first medium of SiO_2 or Si, a ZnO third medium and a SiO_2 second medium stacked in that order. An IDT (interdigital transducer) is disposed along the interface of the first medium and the third medium.

[0004] The vibrational energy of boundary acoustic waves is confined in the third medium made of ZnO in which acoustic velocity becomes low, and thus boundary acoustic waves are propagated. In this device, the IDT is made of A1.

[0005] Patent Document 1 has disclosed a boundary acoustic wave having a multilayer structure including a first medium, a third medium and a second medium stacked in that order as in Non-Patent Document 1. In Patent Document 2, the first medium is made of $LiNbO_3$, the third medium is made of SiO_2, and the second medium is made of SiN. An Al IDT is disposed between the first medium and the third medium. Non-Patent Document 1: IEICE material, 1986, S86-39, pp. 47-4.

Patent Document 1: WO98/52279

Disclosure of Invention

[0006] The boundary acoustic wave devices disclosed in Non-Patent Document 1 and Patent Document 1 each have an Al IDT. In boundary acoustic wave devices using A1 electrodes, the acoustic velocity of transverse waves tends to be higher, and the confinement efficiency of the vibrational energy of the boundary acoustic waves tends to be lower, in comparison with boundary acoustic wave devices using electrodes made of a metal having a higher density than Al, such as Au, Ag, or Cu.

[0007] For developing a boundary acoustic wave device, in general, it has been considered that the confinement of the vibrational energy mainly depends on the third medium in which the acoustic velocity of transverse waves is low, and nobody has thought that confinement of the vibrational energy can be achieved by appropriately selecting the material of electrodes. Accordingly, the confinement efficiency of the vibrational energy is not satisfactory, and the thicknesses of the first and second media are increased. It has been thus considered that boundary acoustic wave devices are difficult to downsize.

[0008] While many of the materials used as the first to third media propagating boundary acoustic waves have negative temperature coefficients of acoustic velocity (TCV), SiO_2 has a positive TCV. Hence, a combination of SiO_2 and a material having a negative TCV can make the TCV value zero or close to zero.

[0009] The frequency temperature coefficient TCF of the boundary acoustic wave device results from the subtraction of the linear expansion coefficient of the boundary wave propagation path from the TCV. Thus, a combination of SiO_2 and another medium material can achieve a boundary acoustic wave device having a low frequency temperature coefficient TCF.

[0010] The IDT of such a known boundary acoustic wave device is made of Al, as described in Non-Patent Document 1 and Patent Document 1. In a structure including a SiO_2 third medium and an Al IDT, the SiO_2 fills the spaces between the Al strips arranged at periodic intervals of the IDT and the reflectors. The difference in density between Al and SiO_2 is small, and the difference in acoustic impedance between them is also small. Accordingly, the reflection of the boundary acoustic waves from the IDT and reflectors is reduced for each A1 strip.

[0011] If the reflection from each of the strips, which are electrode fingers, is reduced, a large number of electrode fingers are required in order for the reflectors to ensure a sufficient reflection coefficient. Accordingly, the reflectors are inevitably formed large, and the resulting boundary acoustic wave device must be large.

[0012] In addition, if the reflection from the IDT is reduced for each strip, the shape factor of a longitudinally coupled resonator-type boundary acoustic wave filter or the directivity of the EWC SPUDT of a transversal boundary acoustic wave filter is degraded, for example.

[0013] In a boundary acoustic wave device having a multilayer structure of second medium/third medium/IDT/first

medium, boundary acoustic waves propagate with the vibrational energy confined in the third medium and the IDT. If the thickness of the third medium is relatively large with the wavelength of propagating boundary waves, higher-order modes are relatively strongly excited. Therefore the thickness of the third medium is preferably smaller than or equal to the wavelength of a single wave of the boundary acoustic waves.

[0014] If the third medium is formed by deposition, such as sputtering, it is difficult to increase the thickness of the third medium to a sufficiently larger value than the thickness of the strips of the IDT and reflectors. A third medium having a small thickness may be cracked due to the unevenness between regions having the strips and regions having no strips.

[0015] Accordingly, an object of the present invention is to provide a boundary acoustic wave device that has a multilayer structure including a first medium, a third medium and a second medium stacked in that order, that can efficiently confine the vibrational energy of boundary acoustic waves in the third medium so as to exhibit a low boundary acoustic wave propagation loss and a high electromechanical coupling coefficient so as not to be affected by higher-order modes to produce undesired spurious responses, and thus can produce superior resonance characteristics or filter properties, and that is not easily cracked in the third medium.

[0016] According to a general aspect of the present invention, a boundary acoustic wave device is provided which has a multilayer structure including a first medium having piezoelectric characteristics, a non-electroconductive second medium, and a third medium through which slow transverse waves propagate at a lower acoustic velocity than slow transverse waves propagating through the first and second media. The first medium, the third medium, and the second medium are stacked in that order. An IDT disposed between the first medium and the third medium. The IDT includes a metal layer made of a metal having a density ρ in the range of 3000 to 21500 kg/m^3. The IDT has electrode fingers at a pitch of λ and has a thickness H1 satisfying the relationship $0.006\lambda \leq H1 \leq 0.2\lambda$, and the third medium has a thickness H2 satisfying the relationship $H1 < H2 \leq 0.7\lambda$.

[0017] In a specific embodiment of the boundary acoustic wave device according to the present invention, the third medium has a thickness H2 satisfying the relationship $H1 < H2 < 0.5\lambda$.

[0018] In another specific embodiment of the boundary acoustic wave device according to the present invention, the third medium is made of SiO_2 or a material mainly containing SiO_2.

[0019] In still another specific embodiment of the boundary acoustic wave device according to the present invention, the first medium is made of $LiNbO_3$ and has Euler angles [ϕ, θ, ψ] satisfying the relationships $-25° < \phi < 25°$, $92° < \theta < 114°$, and $-60° < \psi < 60°$.

[0020] In still another specific embodiment of the boundary acoustic wave device according to the present invention, the first medium is made of $LiNbO_3$ and has Euler angles [ϕ, θ, ψ] satisfying the relationships $-25° < \phi < 25°$, $92° < \theta < 114°$, and $60° < \psi < 120°$.

[0021] In a still further specific embodiment of the boundary acoustic wave device according to the present invention, the first medium is made of $LiNbO_3$ and has Euler angles [ϕ, θ, ϕ] satisfying $-32° < \phi < 32°$, $15° < \theta < 41°$, and $-35° < \psi < 35°$.

[0022] In a still further specific embodiment of the boundary acoustic wave device according to the present invention, the IDT is made of a metal selected from the group consisting of Pt, Au, Cu, Ag, Ni, Ti, Fe, W, Ta, and alloys mainly containing those metals.

[0023] In a still further specific embodiment of the boundary acoustic wave device according to the present invention, the IDT has a structure formed by alternately disposing a first metal layer having a relatively high density and a second metal layer having a relatively low density.

[0024] In a still another specific embodiment of the boundary acoustic wave device of the present invention, the first metal layer is disposed at the first medium side.

[0025] In a still another specific embodiment of the boundary acoustic wave device of the present invention, the first medium and/or the second medium has a multilayer structure including a plurality of medium layers.

[0026] The boundary acoustic wave device of the present invention includes a multilayer structure and an IDT. The multilayer structure includes a first medium having piezoelectric characteristics, a non-electroconductive second medium, and a third medium through which slow transverse waves propagate at a lower acoustic velocity than slow transverse waves propagating through the first and second media. The first medium, the third medium and the second medium are stacked in that order to define the multilayer structure. The IDT is disposed between the first medium and the third medium. Since the IDT is made of a metal having a density ρ in the range of 3000 to 21500 kg/m^3, the propagation loss of boundary acoustic waves can be reduced, and the loss in the boundary acoustic wave device can be reduced.

[0027] Since the thickness H1 of the IDT is in the range of $0.006\lambda \leq H1 \leq 0.2\lambda$, the electromechanical coupling coefficient is sufficient for boundary acoustic waves. Also, the difference in acoustic velocity between SH boundary waves and P+SV boundary waves can be increased. When SH boundary waves are used in the main mode, spuriouses of P+SV boundary waves, which are unnecessary to the SH boundary waves, can be reduced. In addition, since the thickness H2 of the third medium is in the range of $H1 < H2 \leq 0.7\lambda$, higher-order spuriouses of SH boundary waves can also be reduced.

[0028] Thus, the present invention can provide a low-loss boundary acoustic wave device having such a high electromechanical coupling coefficient K^2 that the size, particularly thickness, can be reduced, and exhibiting superior res-

onance characteristics or filter properties.

[0029] If H1 < H2 <0.5λ holds, higher-order spurious responses of SH boundary waves can be more efficiently reduced and more enhanced resonance characteristics or filter properties can be achieved.

[0030] The third medium may be made of SiO_2 or a SiO_2-based material and the SiO_2 has a positive TCV. On the other hand, many of the materials of the media of boundary acoustic wave devices have negative TCV's. Hence, the third medium made of SiO_2 or a SiO_2-based material has a low frequency temperature coefficient TCF and the resulting boundary acoustic wave device can exhibit superior temperature characteristics.

[0031] If the first medium is made of $LiNbO_3$ and has Euler angles ϕ, θ, and ψ in the ranges of $-25° < \phi < 25°$, $92° < \theta < 114°$, and $-60° < \psi < 60°$, the electromechanical coupling coefficient K^2 for P+SV boundary waves can be sufficiently reduced, so that SH boundary waves can be used to achieve superior resonance characteristics or filter properties.

[0032] If the first medium is made of $LiNbO_3$ and has Euler angles ϕ, θ, and ψ in the ranges of $-25° < \phi < 25°$, $92° < \theta < 114°$, and $60° < \psi < 120°$, the electromechanical coupling coefficient K^2 for SH boundary waves can be sufficiently recued, so that P+SV boundary waves can be used to achieve superior resonance characteristics or filter properties.

[0033] If at least one of the second metal layers contains Al, which has a low electrical resistance, the electrical resistance loss due to the electrode fingers can be reduced more effectively.

[0034] If the first medium is made of $LiNbO_3$ and has Euler angles ϕ, θ, and ψ in the ranges of $-32° < \phi < 32°$ $15° < \theta < 41°$, and $-35° < \psi < 35°$, the electromechanical coupling coefficient K^2 for SH boundary waves can be sufficiently reduced, so that P+SV boundary waves can be used to achieve superior resonance characteristic or filter properties.

[0035] The IDT can be made of a metal selected from the group consisting of Pt, Au, Cu, Ag, Ni, Ti, Fe, W, Ta, and alloys mainly containing those metals. Since those metals have higher densities than Al, the propagation loss of boundary acoustic waves can be reduced and thus a low-loss boundary acoustic wave device can be achieved.

[0036] The IDT may be defined by a single metal layer, or a multilayer structure including a first metal layer having a relatively high density and a second metal layer having a relatively low density. If the multilayer structure is formed by alternately disposing the first metal layers and the second metal layers, the thickness of the electrode fingers can be increased on the condition that the propagation loss of boundary acoustic waves is reduced. Thus, the electrical resistance loss due to the electrode fingers can be reduced.

[0037] The first metal layer may be disposed at the first medium side. Hence, the first metal layer having a relatively high density is disposed at the side of the first medium having a low acoustic velocity. Accordingly, a larger amount of energy of boundary acoustic waves is distributed at the first medium side. If the first medium is made of a piezoelectric material, the electromechanical coupling coefficient K^2 can be increased.

[0038] If the first medium and/or the second medium have a multilayer structure defined by a plurality of medium layers including, for example, a compressive stress layer and a tensile stress layer, the total stress can be reduced by the interaction of these stresses. If layers producing different acoustic velocities are stacked in the region in which the vibrational energy of boundary waves exist, the frequency can be controlled by adjusting the thickness of either the first or the second medium by etching, such as ion beam etching. If a plurality of layers each have a sufficiently lower thickness than λ, the multilayer structure can produce an intermediate acoustic velocity for the layers of the multilayer structure.

Brief Description of the Drawings

[0039]

Fig. 1 is a sectional plan view of a boundary acoustic wave device according to an embodiment of the present invention.

Fig. 2 is a sectional front view of a boundary acoustic wave device according to an embodiment of the present invention.

Fig. 3 is a representation of the relationship between the thickness of Au electrodes including the IDT and the acoustic velocity Vm of boundary acoustic waves in a $SiN/SiO_2/IDT/LiNbO_3$ multilayer structure.

Fig. 4 is a representation of the relationship between the thickness of Ag electrodes including the IDT and the acoustic velocity Vm of boundary acoustic waves in a $SiN/SiO_2/IDT/LiNbO_3$ multilayer structure.

Fig. 5 is a representation of the relationship between the thickness of Cu electrodes including the IDT and the acoustic velocity Vm of boundary acoustic waves in a $SiN/SiO_2/IDT/LiNbO_3$ multilayer structure.

Fig. 6 is a representation of the relationship between the thickness of Al electrodes including the IDT and the acoustic velocity Vm of boundary acoustic waves in a $SiN/SiO_2/IDT/LiNbO_3$ multilayer structure.

Fig. 7 is a representation of the relationship between the thickness of Au electrodes including the IDT and the electromechanical coupling coefficient K^2 (%) for boundary acoustic waves in a $SiN/SiO_2/IDT/LiNbO_3$ structure.

Fig. 8 is a representation of the relationship between the thickness of Ag electrodes including the IDT and the electromechanical coupling coefficient K^2 (%) for boundary acoustic waves in a $SiN/SiO_2/IDT/LiNbO_3$ multilayer structure.

Fig. 9 is a representation of the relationship between the thickness of Cu electrodes including the IDT and the electromechanical coupling coefficient K^2 (%) for boundary acoustic waves in a $SiN/SiO_2/IDT/LiNbO_3$ multilayer structure.

Fig. 10 is a representation of the relationship between the thickness of A1 electrodes including the IDT and the electromechanical coupling coefficient K^2 (%) for boundary acoustic waves in a $SiN/SiO_2/IDT/LiNbO_3$ multilayer structure.

Fig. 11 is a representation of the relationship between the thickness of Au electrodes including the IDT and the propagation loss αm (dB/λ) of boundary acoustic waves in a $SiN/SiO_2/IDT/LiNbO_3$ multilayer structure.

Fig. 12 is a representation of the relationship between the thickness of Ag electrodes including the IDT and the propagation loss αm (dB/λ) of boundary acoustic waves in a $SiN/SiO_2/IDT/LiNbO_3$ multilayer structure.

Fig. 13 is a representation of the relationship between the thickness of Cu electrodes including the IDT and the propagation loss αm (dB/λ) of boundary acoustic waves in a $SiN/SiO_2/IDT/LiNbO_3$ multilayer structure.

Fig. 14 is a representation of the relationship between the thickness of Al electrodes including the IDT and the propagation loss αm (dB/λ) of boundary acoustic waves in a $SiN/SiO_2/IDT/LiNbO_3$ multilayer structure.

Fig. 15 is a representation of the relationship between the thickness of Au electrodes including the IDT and the frequency temperature coefficient TCFm (ppm/°C) for boundary acoustic waves in a $SiN/SiO_2/IDT/LiNbO_3$ multilayer structure.

Fig. 16 is a representation of the relationship between the thickness of Ag electrodes including the IDT and the frequency temperature coefficient TCFm (ppm/°C) for boundary acoustic waves in a $SiN/SiO_2/IDT/LiNbO_3$ multilayer structure.

Fig. 17 is a representation of the relationship between the thickness of Cu electrodes including the IDT and the frequency temperature coefficient TCFm (ppm/°C) for boundary acoustic waves in a $SiN/SiO_2/IDT/LiNbO_3$ multilayer structure.

Fig. 18 is a representation of the relationship between the thickness of Al electrodes including the IDT and the frequency temperature coefficient TCFm (ppm/°C) for boundary acoustic waves in a $SiN/SiO_2/IDT/LiNbO_3$ multilayer structure.

Fig. 19 is a representation of the relationship between the thickness of the SiO_2 layer and the primary mode (SHO) and higher-order modes of SH boundary acoustic waves in a $SiN/SiO_2/IDT/LiNbO_3$ multilayer structure in which the IDT is made of A1.

Fig. 20 is a representation of the relationship between the thickness of the SiO_2 layer and the primary mode and higher-order modes of SH boundary acoustic waves in a $SiN/SiO_2/IDT/LiNbO_3$ multilayer structure in which the IDT is made of Au.

Fig. 21 is a representation of the relationship between an Euler angle θ of the $LiNbO_3$ layer and the acoustic velocity Vm (m/s) of boundary acoustic waves in a $SiN/SiO_2/IDT/LiNbO_3$ multilayer structure.

Fig. 22 is a representation of the relationship between an Euler angle θ of the $LiNbO_3$ layer and the electromechanical coupling coefficient K^2 (%) for boundary acoustic waves in a $SiN/SiO_2/IDT/LiNbO_3$ multilayer structure.

Fig. 23 is a representation of the relationship between an Euler angle θ of the $LiNbO_3$ layer and the propagation loss αm (dB/λ) of boundary acoustic waves in a $SiN/SiO_2/IDT/LiNbO_3$ multilayer structure.

Fig. 24 is a representation of the relationship between an Euler angle θ of the $LiNbO_3$ layer and the frequency temperature coefficient TCFm (ppm/°C) for boundary acoustic waves in a $SiN/SiO_2/IDT/LiNbO_3$ multilayer structure.

Fig. 25 is a representation of the relationship between an Euler angle ψ of the $LiNbO_3$ layer and the acoustic velocity Vm (m/s) of boundary acoustic waves in a $SiN/SiO_2/IDT/LiNbO_3$ multilayer structure.

Fig. 26 is a representation of the relationship between an Euler angle ψ of the $LiNbO_3$ layer and the electromechanical coupling coefficient K^2 (%) for boundary acoustic waves in a $SiN/SiO_2/IDT/LiNbO_3$ multilayer structure.

Fig. 27 is a representation of the relationship between an Euler angle ψ of the $LiNbO_3$ layer and the propagation loss αm (dB/λ) of boundary acoustic waves in a $SiN/SiO_2/IDT/LiNbO_3$ multilayer structure.

Fig. 28 is a representation of the relationship between an Euler angle ψ of the $LiNbO_3$ layer and the frequency temperature coefficient TCFm (ppm/°C) for boundary acoustic waves in a $SiN/SiO_2/IDT/LiNbO_3$ multilayer structure.

Fig. 29 is a representation of the relationship between an Euler angle ϕ of the $LiNbO_3$ layer and the acoustic velocity Vm (m/s) of boundary acoustic waves in a $SiN/SiO_2/IDT/LiNbO_3$ multilayer structure.

Fig. 30 is a representation of the relationship between an Euler angle ϕ of the $LiNbO_3$ layer and the electromechanical coupling coefficient K^2 (%) for boundary acoustic waves in a $SiN/SiO_2/IDT/LiNbO_3$ multilayer structure.

Fig. 31 is a representation of the relationship between an Euler angle ϕ of the $LiNbO_3$ layer and the propagation loss αm (dB/λ) of boundary acoustic waves in a $SiN/SiO_2/IDT/LiNbO_3$ multilayer structure.

Fig. 32 is a representation of the relationship between an Euler angle ϕ of the $LiNbO_3$ layer and the frequency temperature coefficient TCFm (ppm/°C) for boundary acoustic waves in a $SiN/SiO_2/IDT/LiNbO_3$ multilayer structure.

Fig. 33 is a representation of the relationship between ψ and the acoustic velocity Vm (m/s) of boundary acoustic waves in a $SiN/SiO_2/IDT/LiNbO_3$ multilayer structure in which the IDT is made of Au and the $LiNbO_3$ substrate has

Euler angles of (0°, 30°, ψ).

Fig. 34 is a representation of the relationship between ψ and the electromechanical coupling coefficient K^2 (%) for boundary acoustic waves in a $SiN/SiO_2/IDT/LiNbO_3$ multilayer structure in which the IDT is made of Au and the $LiNbO_3$ substrate has Euler angles of (0°, 30°, ψ).

Fig. 35 is a representation of the relationship between ψ and the propagation loss αm (dB/λ) of boundary acoustic waves in a $SiN/SiO_2/IDT/LiNbO_3$ multilayer structure in which the IDT is made of Au and the $LiNbO_3$ substrate has Euler angles of (0°, 30°, ψ).

Fig. 36 is a representation of the relationship between ψ and the frequency temperature coefficient TCFm (ppm/°C) for boundary acoustic waves in a $SiN/SiO_2/IDT/LiNbO_3$ multilayer structure in which the IDT is made of Au and the $LiNbO_3$ substrate has Euler angles of (0°, 30°, ψ).

Fig. 37 is a representation of the relationship between ϕ and the acoustic velocity Vm (m/s) of boundary acoustic waves in a $SiN/SiO_2/IDT/LiNbO_3$ multilayer structure in which the IDT is made of Au and the $LiNbO_3$ substrate has Euler angles of (ϕ, 30°, 0°).

Fig. 38 is a representation of the relationship between ϕ and the electromechanical coupling coefficient K^2 (%) for boundary acoustic waves in a $SiN/SiO_2/IDT/LiNbO_3$ multilayer structure in which the IDT is made of Au and the $LiNbO_3$ substrate has Euler angles of (ϕ, 30°, 0°)

Fig. 39 is a representation of the relationship between ϕ and the propagation loss αm (dB/λ) of boundary acoustic waves in a $SiN/SiO_2/IDT/LiNbO_3$ multilayer structure in which the IDT is made of Au and the $LiNbO_3$ substrate has Euler angles of (ϕ, 30°, 0°)

Fig. 40 is a representation of the relationship between ϕ and the frequency temperature coefficient TCFm (ppm/°C) for boundary acoustic waves in a $SiN/SiO_2/IDT/LiNbO_3$ multilayer structure in which the IDT is made of Au and the $LiNbO_3$ substrate has Euler angles of (ϕ, 30°, 0°)

Fig. 41 is a representation of the resonance characteristic of a boundary acoustic wave resonator having a SiN/SiO_2 thickness ratio of 3000 nm/500 nm according to an embodiment of the present invention.

Fig. 42 is a representation of the resonance characteristic of a boundary acoustic wave resonator having a SiN/SiO_2 thickness ratio of 3000 nm/200 nm according to an embodiment of the present invention.

Fig. 43 is a representation of the resonance characteristic of a boundary acoustic wave resonator having a SiN/SiO_2 thickness ratio of 3000 nm/100 nm according to an embodiment of the present invention.

Fig. 44 is a representation of the resonance characteristic of a boundary acoustic wave resonator having a SiN/SiO_2 thickness ratio of PSi/SiO_2 = 3000 nm/500 nm according to an embodiment of the present invention.

Fig. 45 is a representation of the resonance characteristic of a boundary acoustic wave resonator having a SiN/SiO_2 thickness ratio of PSi/SiO_2 = 3000 nm/200 nm according to an embodiment of the present invention.

Fig. 46 is a representation of the resonance characteristic of a boundary acoustic wave resonator having a SiN/SiO_2 thickness ratio of PSi/SiO_2 = 3000 nm/100 nm according to an embodiment of the present invention.

Fig. 47 is a representation of the changes in frequency temperature coefficient TCF (ppm/°C) with SiO_2 thickness in a SiN/SiO_2 /IDT/$LiNbO_3$ multilayer structure.

Fig. 48 is a representation of the changes in frequency temperature coefficient TCF (ppm/°C) with SiO_2 thickness in a PSi/SiO_2 /IDT/$LiNbO_3$ multilayer structure.

Fig. 49 is a representation of the displacement distribution of SH boundary acoustic waves and P and SV wave components in a structure of SiN/SiO_2/IDT/15° Y-cut X-propagating $LiNbO_3$ substrate including a 0.05λ thick Al IDT and a 0.5λ thick SiO_2 layer.

Fig. 50 is a representation of the displacement distribution of SH boundary acoustic waves and P and SV wave components in a structure of SiN/SiO_2/IDT/15° Y-cut X-propagating $LiNbO_3$ substrate including a 0.10λ thick Al IDT and a 0.5λ thick SiO_2 layer.

Fig. 51 is a representation of the displacement distribution of SH boundary acoustic waves and P and SV wave components in a structure of SiN/SiO_2/IDT/15° Y-cut X-propagating $LiNbO_3$ substrate including a 0.05λ thick Au IDT and a 0.5λ thick SiO_2 layer.

Reference Numerals

[0040]

10	boundary acoustic wave device
11	first medium
12	second medium
13	third medium
14	IDT
14a, 14b	electrode fingers

15, 16 reflector

Best Mode for Carrying Out the Invention

[0041] The present invention will become clear from the description of specific embodiments of the present invention with reference to the drawings.

[0042] In the Description, the Euler angles, the crystallographic axis, and equivalent Euler angles refer to the following.

Euler Angles

[0043] In the Description, the Euler angles (ϕ, θ, ψ) representing the direction of the cut surface of the substrate and the propagation direction of the boundary waves are based on the right-handed Euler angles described in a document "Danseiha Soshi Gijutsu Handbook (Acoustic Wave Device Technology Handbook)" (Japan Society for the Promotion of Science, Acoustic Wave Device Technology the 150th Committee, 1st Version 1st printing, published on January 30, 2001, p. 549). Specifically, in LN crystallographic axes X, Y, and Z, the X axis is rotated ϕ turn anticlockwise about the Z axis to define a Xa axis. Subsequently, the Z axis is rotated θ turn anticlockwise about the Xa axis to define a Z' axis. A plane including the Xa axis whose normal is the Z' axis is defined as the cut surface. The propagation direction of the boundary waves is set to be the direction of the X' axis that is defined by rotating the Xa axis ψ turn anticlockwise about the Z' axis.

Crystallographic Axis

[0044] As for the $LiNbO_3$ crystallographic axes X, Y, and Z defining the initial Euler angles, the Z axis is set to be parallel to the c axis, the X axis is set to be parallel to one of the equivalent a axes extending in three directions, and the Y axis is set to be the normal of a plane including the X axis and the Z axis.

Equivalent Euler Angles

[0045] The present invention requires only that the $LiNbO_3$ Euler angles (ϕ, θ, ψ) be crystallographically equivalent. For example, a document (Nihon Onkyo Gakkai-shi (Journal of the Acoustical Society of Japan) Vol. 36, No. 3, 1980, pp. 140-145) has taught that $LiNbO_3$ belongs to the trigonal 3m point group, and Equation [4] therefore holds.

$$\begin{aligned} F(\phi, \theta, \psi) &= F(60^\circ - \phi, -\theta, \psi) \\ &= F(60^\circ + \phi, -\theta, 180^\circ - \psi) \\ &= F(\phi, 180^\circ + \theta, 180^\circ - \psi) \\ &= F(\phi, \theta, 180^\circ + \psi) \end{aligned} \quad [4]$$

[0046] In the equation, F represents a boundary wave property, such as electromechanical coupling coefficient k_s^2, propagation loss, TCF, PFA, or a natural unidirectional property. For example, when the propagation direction is reversed, the PFA natural unidirectional properties are changed in plus/minus sign, but their absolute values do not change; hence they are estimated to be practically equivalent. Although Document 7 has discussed surface waves, the same applies to the boundary waves in terms of crystalline symmetry.

[0047] For example, the propagation characteristics of boundary waves with Euler angles of (30°, θ, ψ) are equivalent to those of boundary waves with Euler angles of (90°, 180°-θ, 180°-ψ). For example, the propagation characteristics of boundary waves with Euler angles (30°, 90°, 45°) are equivalent to those of boundary waves with Euler angles shown in Table 1.

[0048] Although the constants of conductive material used for the calculations in the present invention are those of polycrystals, epitaxial films or the like can also produce boundary wave propagation characteristics to the extent that problems do not occur in practice according to Equation [4] because the crystal orientation dependence of the substrate is more dominant to the boundary wave characteristics than the crystal orientation dependence of the layers.

[Table 1]

ϕ (°)	θ (°)	ψ (°)
30	90	225
30	270	135
30	270	315
90	90	135
90	90	315
90	270	45
90	270	225
150	90	45
150	90	225
150	270	135
150	270	315
210	90	135
210	90	315
210	270	45
210	270	225
270	90	45
270	90	225
270	270	135
270	270	315
330	90	135
330	90	315
330	270	45
330	270	225

[0049] Fig. 1 is a schematic sectional plan view showing the structure of the electrodes of a boundary acoustic wave device according to an embodiment of the present invention, and Fig. 2 is a sectional front view of the boundary acoustic wave device.

[0050] The boundary acoustic wave device 10 of the present embodiment includes a third medium 13 and a second medium 12 formed in that order on a first medium 11 having piezoelectric characteristics. An IDT 14 and reflectors 15 and 16 are disposed along the interface between the first medium 11 and the third medium 13. In other words, electrodes are disposed along the interface between the first and third media 11 and 13.

[0051] The IDT 14 has a plurality of electrode fingers 14a and a plurality of electrode fingers 14b that are alternately disposed between other electrode fingers. The electrode fingers 14a are electrically connected to one bus bar, and the other electrode fingers 14b are electrically connected to the other bus bar. In the present embodiment, the IDT 14 is weighted by varying the finger overlap.

[0052] The reflectors 15 and 16 are disposed outside the direction perpendicular to the direction in which the fingers 14a and 14b of the IDT 14 extend, that is, at both sides of the direction at which boundary acoustic waves propagate. The IDTs 15 and 16 each have a plurality of electrode fingers extending in the direction perpendicular to the direction in which the boundary acoustic waves propagate, and the ends of these electrode fingers are closed together. While the ends of the reflectors are closed together in the embodiment, OPEN reflectors having open ends may be used.

[0053] In the boundary acoustic wave device 10, the third medium 13 in which slow transverse waves used in the device have a relatively low acoustic velocity is disposed between the first and second media 11 and 12 in which the slow transverse waves have relatively high acoustic velocities. Consequently, boundary acoustic waves are propagated while their vibrational energy is confined in the third medium 13 exhibiting a relatively low acoustic velocity. More specifically, boundary acoustic waves are propagated in the direction perpendicular to the electrode fingers 14a and 14b

and parallel to the plane on which the IDT 14 is formed, by confining the vibrational energy of the boundary acoustic waves between the interface of the second and third media 12 and 13 and the interface of the first and third media 11 and 13.

[0054] In the present embodiment, the first medium 11 is made of piezoelectric 15° Y-cut X-propagating $LiNbO_3$ having Euler angles of (0°, 105°, 0°). The second medium 12 is made of non-electroconductive SiN. The third medium 13 is made of SiO_2.

[0055] The IDT 14 and the reflectors 15 and 16 are made of a metal having a higher density than A1. More specifically, the IDT 14 is made of a metal having a density ρ in the range of 3000 to 21500 kg/m^3. The IDT 14 has a thickness H1 in the range of $0.006\lambda \leq H1 \leq 0.2\lambda$ and the third medium 13 has a thickness H2 in the range of $H1 < H2 \leq 0.7\lambda$, where λ represents the pitch of electrode fingers of the IDT 14. Thus, the boundary acoustic wave device 10 can exhibit low loss characteristics and can be downsized. The boundary acoustic wave device 10 also has a high electromechanical coupling coefficient K^2 for boundary acoustic waves and is accordingly not affected by higher-order spurious responses, thus exhibiting superior characteristics. This is further described with reference to specific experiments.

[0056] The relationships of the thickness of the electrodes of the boundary acoustic wave device with the acoustic velocity of boundary acoustic waves, the electromechanical coupling coefficient K, the propagation loss αm, and the frequency temperature coefficient TCF were evaluated. For the evaluation, the electrodes were formed of Al, which is conventionally used as the electrode material of the IDT, or Cu, Ag or Au that has a higher density than A1. The results are shown in Figs. 3 to 18.

[0057] For obtaining the results shown in Figs. 3 to 18 in the SiN/SiO_2/IDT/15° Y-cut X-propagating $LiNbO_3$ multilayer structure, the thickness of the third medium or the SiO_2 layer was set at 0.5λ, and the thicknesses of the first and second media were set infinite. In Figs. 3 to 18, U2 shows the results for boundary acoustic waves essentially composed of SH waves, and U3 shows the results for boundary acoustic waves essentially composed of P+SV components.

[0058] In the 15° Y-cut X-propagating $LiNbO_3$ substrate having Euler angles of (0°, 105°,0°), the coupling of SV+P boundary acoustic waves with the piezoelectric characteristics is weak. Accordingly, the SV+P boundary waves are hardly excited, and SH boundary waves are used as boundary acoustic waves in the main mode.

[0059] The results shown in Figs. 3 to 18 were calculated according to a method disclosed in "A method for estimating optimal cuts and propagation directions for excitation and propagation directions for excitation of piezoelectric surface waves" (J. J. Campbell and W. R. Jones, IEEE Trans. Sonics and Ultrason., Vol. SU-15 (1968) pp. 209-217).

[0060] When the boundaries were open, the acoustic velocity and the propagation loss were obtained, assuming that the displacement, the potential, the normal component of electric flux density, and the vertical stress at the boundary between the second medium 12 and the third medium 13, the boundary between the third medium 13 and the IDT 14, and the boundary between the IDT 14 and the first medium 11 were continuous, that the thicknesses of the second medium 12 and the first medium 11 were infinite, and that the conductor, or the IDT electrode 14, had a relative dielectric constant of 1. When the boundaries were closed, the acoustic velocity and the propagation loss were obtained, assuming that the potentials at the boundary between the third medium 13 and the IDT 14 and the boundary between the IDT 14 and the first medium 11 were 0. The electromechanical coupling coefficient K^2 was derived from Equation (1). In Equation (1), Vf represents the acoustic velocity at an open boundary, and V represents the acoustic velocity at a closed boundary.

$$K^2 = 2 \times |Vf - V|/Vf \qquad \text{Equation (1)}$$

[0061] The frequency temperature coefficient TCF was obtained from the following Equation (2) depending on the phase velocity V at 20°C, 25°C, and 30°C.

$$TCF = (V[30°C]-V[20°C])/V[25°C]/10°C - \alpha s \qquad (2)$$

[0062] αS represents the linear expansion coefficient of the first medium 11 in the direction in which boundary acoustic waves propagate.

[0063] The power flow angle (PFA) at Euler angles [ϕ, 0, ψ] was derived from the following Equation (3) using the phase velocities V at ψ - 0.5°, ψ, and ψ + 0.5°

$$PFA = \tan^{-1}\{V[\psi] \times (V[\psi + 0.5°] - V[\psi - 0.5°])\} \qquad (3)$$

[0064] The acoustic velocities of longitudinal waves, fast transverse waves and slow transverse waves in a Y-rotated X-propagating $LiNbO_3$ are 6547, 4752 and 4031 m/s, respectively. The acoustic velocities of longitudinal waves and slow transverse waves in the SiO_2 layer are 5960 and 3757 m/s, respectively. The acoustic velocities of longitudinal waves and slow transverse waves in the SiN layer are 10642 and 5973 m/s, respectively.

[0065] Figs. 3 to 6 and Figs. 11 to 14 show that in any case using different metal electrodes, the propagation loss αm of SH boundary waves is 0 at a thickness at which the acoustic velocity of SH boundary acoustic waves is less than or equal to the lowest value 4031 m/s of the acoustic velocities of longitudinal waves, fast transverse waves and slow transverse waves.

[0066] Since Al has a relatively low density ρ, the acoustic velocity of boundary acoustic waves is 4031 m/s or less. In order to reduce the propagation loss αm to 0, the thickness of A1 electrodes must be large. On the other hand, electrodes made of Cu, Ag, or Au, which has a higher density than Al, can lead to a propagation loss αm of 0 by using thinner IDT than the Al IDT. Figs. 3 to 6 show that as the density of the electrodes is increased, the acoustic velocities of SH boundary waves and P+SV boundary waves can more largely differ from each other in the range of electrode thicknesses at which the propagation loss $\alpha m = 0$ holds. However, in use of Al electrodes, there is not the difference.

[0067] A lager thickness of the electrodes increases the difference in height between the regions where the electrode fingers of the IDT 14 and reflectors 15 and 16 are present and the regions where the electrode fingers are not present. Accordingly, if the third medium 13 and the second medium 12 are formed by sputtering or evaporation in the portions of medium in which the IDT 14 and reflectors 15 and 16 are arranged, their coverage is not sufficient and the third medium 13 and the second medium 12 may be cracked. In addition, the deposition time is increased, and consequently the cost for forming the third medium 13 and the second medium 12 is liable to increase.

[0068] In contrast, Cu, Ag and Au having higher densities than Al can lead to electrodes with a small thickness, and accordingly can solve the above problems. Figs. 3 to 6 show that there is a condition that the acoustic velocities of SH boundary waves and P+SV boundary waves can more largely differ from each other in the range of electrode thicknesses at which the propagation loss $\alpha m = 0$ holds as the density of the electrodes is increased, and that however there is not such a condition in use of A1. In use of SH boundary waves as the main mode, therefore, spurious responses of the P+SV boundary waves acting as unnecessary modes can be reduced by forming the electrodes of a metal having a higher density than Al to a thickness in the range of 0.006λ to 0.2λ.

[0069] As is clear from Figs. 7 to 10, the use of a conductive material having a relatively high density can produce a higher electromechanical coupling coefficient K^2. An IDT 14 made of a conductive material having a high density concentrates the vibrational energy in the vicinity of the IDT 14 because the acoustic velocity in the conductive material is very low. In addition, if the first medium 11 is formed of a piezoelectric material with the IDT 14 in contact with the piezoelectric material, the energy in the piezoelectric material is increased and thus the electromechanical coupling coefficient K^2 is further increased.

[0070] A design technique for adjusting the electromechanical coupling coefficient K^2 with propagation angle has been known. If the electromechanical coupling coefficient K^2 is increased, the range of its adjustment expands. Accordingly, the range of design can be further increased.

[0071] Pt electrodes resulted in substantially the same effect as the Au electrodes. Since Pt has a slightly higher density than Au, the vibrational energy tended to concentrate more in the vicinity of the IDT 14.

[0072] Figs. 49 to 51 show displacement distributions of SH boundary acoustic waves in use of an IDT 14 defined by a 0.05λ thick Al layer, a 0.10λ thick Al layer, or a 0.05λ thick Au layer. In the use of the 0.05λ thick Al IDT 14, the vibrational energy is emitted to the $LiNbO_3$ side or first medium side as is clear from Fig. 49, and hence boundary acoustic waves are not sufficiently confined in the boundaries between the media. In the use of the 0.10λ thick Al IDT 14, the vibrational energy is prevented from emitting, but is distributed in the $LiNbO_3$ layer of the first medium 11 up to a depth of 5λ or more (not shown in the figure) and in the SiN layer of the second medium up to a depth of about 1.2λ, as is clear from Fig. 50. Thus, the results suggest that the thicknesses of the first and second media must be large.

[0073] On the other hand, in the use of the 0.05λ thick Au IDT 14 as shown in Fig. 51, the vibrational energy is distributed only in the region of the $LiNbO_3$ layer up to a depth of 0.9λ and the region of the SiN layer up to a depth of 0.9λ even though the IDT thickness is as small as 0.05λ. Hence the vibrational energy of boundary waves can be efficiently confined. The use of an IDT 14 made of Au having a higher density ρ than Al allows the reduction of the thicknesses of both the SiN second medium and the $LiNbO_3$ first medium. Consequently, the resulting boundary acoustic wave device can be thin and its manufacturing cost can be reduced.

[0074] SiO_2 has a density of 2210 kg/m^3, and an acoustic characteristic impedance of 8.3×10^6 kg·s/m^2 for transverse waves; Al has a density of 2699 kg/m^3, and an acoustic characteristic impedance of 8.4×10^6 kg·s/m^2 for transverse waves; Cu has a density of 8939 kg/m^3, and an acoustic characteristic impedance of 21.4×10^6 kg·s/m^2 for transverse waves; Ag has a density of 10500 kg/m^3, and an acoustic characteristic impedance of 18.6×10^6 kg·s/m^2 for transverse waves; Au has a density of 19300 kg/m^3, and an acoustic characteristic impedance of 24.0×10^6 kg·s/m^2 for transverse waves.

[0075] Since the differences in density and acoustic characteristic impedance between SiO_2 and Al are small, the

strips have a low reflection coefficient in the structure including a SiO_2 third medium 13 and an Al IDT 14. Accordingly, a large number of strips are required in order to ensure a sufficient reflection coefficient of the reflectors 15 and 16. This disadvantageously increases the size of the device. If the reflection of the strips of the IDT 14 is reduced, the shape factor of a longitudinally coupled resonator-type boundary acoustic wave filter or the directivity of the EWC SPUDT of a transversal boundary acoustic wave filter is disadvantageously degraded.

[0076] In contrast, the difference in density and acoustic characteristic impedance between SiO_2 and Au are sufficiently large. Accordingly, the strips of the IDT 14 have a sufficiently high reflection coefficient in the structure including a SiO_2 third medium 13 and a Au IDT 14. The reflectors 15 and 16 also have a sufficiently high reflection coefficient even if the number of strips is small. Consequently, a longitudinally coupled resonator-type filter having a superior shape factor, or a SPUDT having a high directivity can be achieved.

[0077] In the boundary acoustic wave device 10 of the above embodiment, the third medium 13 has a certain thickness, and the interface between the second medium 12 and the third medium 13 and the interface between the third medium 13 and the first medium 11 are formed on and under the third medium 13. If the thickness of the third medium 13 is increased, a higher-order mode occurs in which waves propagates with confinement between those interfaces.

[0078] As described above, in the $LiNbO_3$ substrate having Euler angles (0°, 105°, 0°), SV+P boundary waves are hardly excited and SH boundary waves act as the main mode. Also, an SH component-based higher-order mode is strongly excited to cause spurious response. It is accordingly important to reduce such an SH-type higher-order mode. In a boundary acoustic wave device having the multilayer structure including the above three media 11 to 13, higher-order waves propagating with being confined between the interfaces on and under the third medium 13 can be cut off to reduce the higher-order waves by reducing the thickness of the third medium 13.

[0079] Figs. 19 and 20 are each a representation of the relationship between higher order modes and the thickness of the SiO_2 layer of a $SiN/SiO_2/IDT/LiNbO_3$ multilayer structure including an Al IDT or Au IDT. In the multilayer stricter, the $LiNbO_3$ layer had Euler angles of (0°, 105°, 0°) and the IDT had a thickness of 0.05λ.

[0080] Fig. 19 clearly shows that when the SiO_2 layer has a thickness of 0.9λ or less in the structure having the Al IDT, higher order SH boundary wave spuriouses are cut off. On the other hand, when the SiO_2 layer has a thickness of 0.7λ or less in the structure having the Au IDT, higher-order SH boundary waves can be cut off, as shown in Fig. 20. Thus, the use of high-density Au electrodes allows the thickness of the SiO_2 layer or third medium 13, which can cut off higher mode waves, to be reduced. Accordingly, the boundary acoustic wave device can be downsized.

[0081] This is because in use of a high-density conductive material, the vibrational energy is easily concentrated in the vicinities of the third medium 13 and the IDT 14 to produce higher order modes, and is because it is accordingly desirable that the thickness of the third medium 13 be reduced. Fig. 20 clearly shows that a third medium 13 with a smaller thickness allows the acoustic velocity of the main-mode waves SHO to differ largely from that of higher-order waves designated by, for example, SH1. Thus, the difference in frequency between the main mode and higher modes can advantageously be increased.

[0082] In use of an IDT 14 made of Au or a metal having a higher density than A1, higher order modes can be cut off by setting the thickness of the third medium 13 to 0.7λ or less, as is clear from Fig. 20. Furthermore, in order to adapt to variations in manufacture or in order to cut off higher order modes from a wide range of frequency bands, the third medium 13 preferably has a thickness of 0.5λ or less.

[0083] The case in which SH boundary waves are in the main mode has been described above. If P+SV boundary waves are in the main mode, P+SV higher order modes are strongly excited. Accordingly, the P+SV higher-order modes must be reduced. The P+SV higher order modes can be reduced by reducing the thickness of the third medium 13, as in the case of the higher order SH boundary waves. In addition, the difference in response frequency between higher order modes and the main mode can be increased.

[0084] In use of P+SV boundary waves, the difference in response frequency between the main mode and higher order modes can be sufficiently increased by reducing the thickness of the third medium 13 to 0.7λ or less, preferably to 0.5λ or less.

[0085] Main mode P+SV boundary waves can be easily produced by using, for example, a 120° Y-cut X-propagating $LiNbO_3$ substrate having Euler angles of (0°,30°, 0°).

[0086] Figs. 21 to 24 show the relationships of θ of the Euler angles (0°, θ, 0°) of the $LiNbO_3$ first medium 11 with the acoustic velocity of boundary acoustic waves, the electromechanical coupling coefficient K^2, the propagation loss, and the frequency temperature coefficient TCF, respectively. In Figs. 21 to 24, U2 shows the results for boundary waves essentially composed of SH components, and U3 shows the results for boundary waves essentially composed of P+SV components. The results were obtained under the following conditions.

[0087] Multilayer structure: $SiN/SiO_2/IDT/LiNbO_3$, where the $LiNbO_3$ is the first medium 11; the SiN is the second medium 12; and the SiO_2 is the third medium 13.

[0088] The thickness of the SiN second medium 12 was infinite, the thickness of the first medium 11 was infinite, the thickness of the SiO_2 third medium 13 was 0.5λ; and the IDT 14 was formed of Au to a thickness of 0.07λ.

[0089] As is clear from Figs. 21 to 24, when an Euler angle θ is about 114°, the spuriouses of P+SV boundary waves

are reduced and the electromechanical coupling coefficient K^2 for SH boundary waves is increased.

[0090] More specifically, when the Euler angle θ is preferably in the range of $92° > \theta > 114°$, the electromechanical coupling coefficient K^2 for P+SV boundary waves is reduced to 1% or less; and more preferably when the Euler angle θ is in the range of $96° > \theta > 111°$, the electromechanical coupling coefficient K^2 for P+SV boundary waves is reduced to 0.5% or more. Still more preferably, when $100° > \theta > 108°$ holds, the electromechanical coupling coefficient K^2 for P+SV boundary waves is reduced to 0.1% or less; and further, when $\theta = 104°$ holds, the electromechanical coupling coefficient K^2 for P+SV boundary waves comes to 0 or an optimum and the electromechanical coupling coefficient K^2 for SH boundary waves is increase to 14%.

[0091] Figs. 25 to 28 are representations of the relationships of ψ of the Euler angles (00, 104°,ψ) with the acoustic velocity of boundary acoustic waves, the electromechanical coupling coefficient K^2, the propagation loss, and the frequency temperature coefficient TCF, respectively, obtained in the same manner as Figs. 21 to 24.

[0092] The Euler angle ψ represents the direction in which boundary acoustic waves propagate on the substrate.

[0093] As is clear from Figs. 25 to 28, the electromechanical coupling coefficient for SH boundary waves can be adjusted in the range of 0.1% to 17.8% by setting the Euler angle ψ in the range of 0° to 60°. In this vicinity, the electromechanical coupling coefficient K^2 for P+SV boundary waves, which cause spuriouses, is as small as about 0% at $\psi = 0°$, 0.4% at $\psi = 30°$, 0.7% at $\psi = 40°$, and 1.4% at $\psi = 50°$.

[0094] If ψ is larger than 60°, the electromechanical coupling coefficient K^2 for P+SV waves becomes 2.6% or more and the electromechanical coupling coefficient K^2 for SH boundary waves becomes as small as 0.1% or less. Thus, P+SV boundary waves can be used as the main mode.

[0095] Figs. 29 to 32 are representations of the relationships of ϕ of the Euler angles (ϕ, 104°, 0°) with the acoustic velocity of boundary acoustic waves, the electromechanical coupling coefficient K^2, the propagation loss, and the frequency temperature coefficient TCF, respectively, obtained in the same manner as Figs. 21 to 24.

[0096] Figs. 29 to 32 and crystalline symmetry show that when the Euler angle is in the ranges of $-25° > \phi > 25°$ and $95° > \phi > 145°$, the electromechanical coupling coefficient K^2 for P+SV boundary waves is advantageously reduced to 1% or less; and when the Euler angle ϕ is in the ranges of $-19° > \phi > 19°$ and $101° > \phi > 139°$, the electromechanical coupling coefficient K^2 for P+SV boundary waves is more advantageously reduced to 0.5% or less. Still more advantageously, when ϕ is in the ranges of $-8° > \phi > 8°$ and $112° > \phi > 128°$, the electromechanical coupling coefficient K^2 for P+SV boundary waves is reduced to 0.1% or less; and further, when the Euler angle is $\phi = 0°$ or $\phi = 120°$, the electromechanical coupling coefficient K^2 for P+SV boundary waves comes to about 0% or an optimum and the electromechanical coupling coefficient K^2 for SH boundary waves is increased to 16.7% or more.

[0097] Figs. 21 to 24 also show that in the vicinity of $\theta = 30°$, spuriouses of SH boundary waves are reduced and the electromechanical coupling coefficient K^2 for P+SV boundary waves is increased.

[0098] It is shown that the electromechanical coupling coefficient K^2 for SH boundary waves is reduced to 1% or less at an Euler angle θ in the range of $15° > \theta > 41°$ and is more advantageously reduced to 0.5% or less at an Euler angle θ in the range of $21° > \theta > 38°$.

[0099] It is further shown that the electromechanical coupling coefficient K^2 for SH boundary waves is still more advantageously reduced to 0.1% or less in the range of $26° > \theta > 34°$, and that when the Euler angle is $\theta = 30°$, the electromechanical coupling coefficient K^2 for SH boundary waves comes to about 0% or an optimum and the electromechanical coupling coefficient K^2 of P+SV boundary waves is increase to 4% or more.

[0100] Figs. 33 to 36 are representations of the relationships of ψ of the Euler angles (0°, 30°, ψ) with the acoustic velocity of boundary acoustic waves, K^2, the propagation loss, and the frequency temperature coefficient TCF, respectively, obtained in the same manner as Figs. 21 to 24,

[0101] Figs. 33 to 36 and crystalline symmetry show that when the Euler angle ψ is in the range of $-35° > \psi > 35°$, the electromechanical coupling coefficient K^2 for SH boundary waves is reduced to 1% or less; and when $-20° > \psi > 20°$ holds, the electromechanical coupling coefficient K^2 for SH boundary waves is advantageously reduced to 0.5% or less. Still more advantageously, the electromechanical coupling coefficient K2 for SH boundary waves is reduced to 0.1% or less in the range of $-8° > \psi > 8°$. Furthermore, when the Euler angle is $\psi = 0°$, the electromechanical coupling coefficient K^2 for SH boundary waves comes to about 0% or an optimum and the electromechanical coupling coefficient K^2 of P+SV boundary waves is increased to 4.4% or more.

[0102] In use of P+SV boundary waves in the vicinity of the Euler angles (0°, 30°, 0°), an propagation angle ψ of 35° or more leads to an increased electromechanical coupling coefficient K^2 for SH boundary waves, consequently causing spurious responses. However, if the spurious responses are acceptable in view of designing the product, the electromechanical coupling coefficient K^2 can be adjusted with the propagation angle ψ, as in the case in which SH boundary waves are used as the main mode.

[0103] Figs. 37 to 40 are representations of the relationships of ϕ of the Euler angles (ϕ, 30°, 0°) with the acoustic velocity of boundary acoustic waves, the electromechanical coupling coefficient K^2, the propagation loss, and the frequency temperature coefficient TCF, respectively, obtained in the same manner as Figs. 21 to 24.

[0104] Figs. 37 to 40 and crystalline symmetry show that when the Euler angle ϕ is in the ranges of $-32° > \phi > 32°$ and

88° > ϕ > 152°, the electromechanical coupling coefficient K^2 for SH boundary waves is reduced to 1% or less; and when the Euler angle is in the ranges of -21° > ϕ > 21° and 95° > ϕ > 145°, the electromechanical coupling coefficient K^2 for SH boundary waves is advantageously reduced to 0.5% or less. Still more advantageously, the electromechanical coupling coefficient K^2 for SH boundary waves is reduced to 0.1% or less in the ranges of -9° > ϕ > 9° and 111° > ϕ > 129°; and further, when the Euler angle ϕ is ϕ = 0° or ϕ = 120°, the electromechanical coupling coefficient K^2 for SH boundary waves comes to about 0% or an optimum and the electromechanical coupling coefficient K^2 of P+SV boundary waves is increased to 3.9% or more.

[0105] The IDT electrode may include first metal layers having a relatively high density and second metal layers having a relatively low density that are alternately stacked one on top of another. An Al layer may be added to the stack of the metal layers, as long as the stack includes at least one layer of a metal having a density of 3000 to 21500 kg/m^3.

[0106] Figs. 41 to 46 are representations of the measurement results of the resonance characteristics of the boundary acoustic wave device 10 according to the embodiment above. Figs. 47 and 48 are representations of the measurement results of frequency temperature coefficient.

[0107] The boundary acoustic wave devices that produced the results shown in Figs. 41 to 46 and Figs. 47 and 48 had the following structure:

First medium 11: $LiNbO_3$ with a thickness of 370 μm;
Third medium 13: SiO_2 with a thickness of 100 nm, 200 nm, or 500 nm;
Second medium 12: SiN or poly Si (PSi) with a thickness of 3.0 μm; and
IDT 14: having a multilayer structure of five layers: Al/Ti/Ni/Au/Ni with thicknesses of 100/10/10/45/10 nm, respectively.

[0108] The IDT 14 had 60 pairs of electrode fingers, and the reflectors 15 and 16 had 51 electrode fingers. The overlap of the IDT 14 was 30λ and the aperture width was 30.4λ. The IDT 14 was weighted by varying the finger overlap such that the center overlap was 30λ and the overlap at both ends in the direction in which boundary acoustic waves propagate was 15λ.

[0109] The distance between the centers of electrode fingers between the IDT 14 and the reflectors 15 and 16 was 1.6 μm and the pitch of the electrode fingers of the IDT 14 and the reflectors 15 and 16 was 0.8 μm. The electrode fingers had a line width of 0.4 μm, and the spaces between the electrode fingers were 0.4 μm in the direction in which boundary waves propagate.

[0110] Figs. 41 to 43 and 47 show the results of a structure including a SiN second medium 12, and Figs. 44 to 46 and 48 show the results of a structure including a PSi second medium 12.

[0111] As is clear from Figs. 41 to 46, superior resonance characteristics can be obtained in both cases in which the thicknesses of the SiO_2 layer and the SiN layer are varied and in which the thicknesses of the SiO_2 layer and the poly Si (PSi) layer are varied.

[0112] As is clear from Figs. 47 and 48, the resonant frequency temperature characteristics and the antiresonant frequency temperature characteristics (TCF) are controlled by varying the thickness of the SiO_2 layer. In particular, the absolute value of the frequency temperature coefficient TCF can be advantageously reduced by increasing the thickness of the SiO_2 layer.

[0113] The present invention is not limited to the boundary acoustic wave resonator having the electrode structure shown in Fig. 1, and may be applied to other boundary acoustic wave resonators having other electrode structures. The invention is not also limited to resonators, and may be applied to a variety of filter devices using boundary acoustic waves, such as ladder-type filters, longitudinally coupled resonator filters, laterally coupled resonator filters, transversal filters, and boundary acoustic wave optical filters, and further applied to switching elements, such as boundary acoustic wave optical switches.

[0114] The material of the electrodes is not limited to Pt, Au, Ag, and Cu, and other metals having a higher density ρ than A1 can be used, such as Ni, Ti, Fe, W, and Ta. The electrodes may include an additional thin layer made of a metal exhibiting high adhesion, such as Ti, Cr, NiCr, or Ni at the medium side to increase the adhesion to the mediums or the electric power resistance. Alternatively, the electrodes, such as the IDT 14, may have a multilayer structure including metal layers, and such a thin adhesion layer may be disposed between the metal layers.

[0115] If the IDT 14 is formed of a conductive material having a high density for a frequency band of over 1 GHz, the conductive material for the IDT may be formed to an excessively small thickness, and the electrode finger strips can have a high resistance. For this disadvantage, the resistance of the electrode can be reduced by forming a multilayer structure of second medium/third medium/multilayer metal IDT/first medium including the multilayer IDT of a low-density conductive material and a high-density conductive material, such as Al and Au.

[0116] In addition, high-density metals help vibrational energy concentrate in the vicinity of the IDT. Accordingly, the electromechanical coupling coefficient can be increased and thus the same effects as in the above embodiment can be produced.

[0117] Before forming the second medium and the third medium, the thickness of the IDT may be adjusted to control the frequency by a variety of techniques, such as reverse sputtering, ion beam milling, reactive ion etching, and wet etching.

[0118] The thickness of the third medium may be further reduced by milling, etching or the like, or may be increased by deposition, such as sputtering or evaporation, and thus the frequency can be controlled.

[0119] The first to third media 11 to 13 may be formed of various types of materials including insulating materials and piezoelectric materials, such as Si, glass, SiO_2, SiC, ZnO, Ta_2O_5, lead zirconate titanate ceramic, AlN, Al_2N, Al_2O_3, $LiTaO_3$, and KN, without being limited to the above-described materials.

[0120] The media may each have a multilayer structure composed of a plurality of media. In the present invention, it is preferable that the acoustic velocity in the IDT 14 be much lower than that in the third medium.

[0121] If the third medium 13 or first medium 11 in contact with the IDT 14 has piezoelectric characteristics, the electromechanical coupling coefficient K^2 for boundary acoustic waves can be advantageously increased.

[0122] A protective layer for preventing corrosive gases from permeating may be provided outside the first medium 11/IDT/piezoelectric material structure to enhance the strength of the boundary acoustic wave device. The boundary acoustic wave device may be enclosed in a package in some cases. The protective layer is not particularly limited, and can be made of a synthetic resin, such as polyimide resin or epoxy resin, an inorganic insulating material, such as titanium oxide, aluminium nitride or aluminium oxide, or a metal, such as Au, A1 or W.

Claims

1. A boundary acoustic wave device comprising:

   a multilayer structure including a first medium having piezoelectric characteristics, a non-electroconductive second medium, and a third medium through which slow transverse waves propagate at a lower acoustic velocity than slow transverse waves propagating through the first and second media, the first medium, the third medium and the second medium being stacked in that order; and
   an IDT disposed between the first medium and the third medium,

   wherein the IDT includes a metal layer made of a metal having a density ρ in the range of 3000 to 21500 kg/m, and the IDT has electrode fingers at a pitch of λ and has a thickness H1 satisfying the relationship $0.006\lambda \leq H1 \leq 0.2\lambda$, and the third medium has a thickness H2 satisfying the relationship $H1 < H2 \leq 0.7\lambda$.

2. The boundary acoustic wave device according to Claim 1, wherein the thickness H2 of the third medium satisfies the relationship $H1 < H2 < 0.5\lambda$.

3. The boundary acoustic wave device according to Claim 1 or 2, wherein the third medium is made of SiO_2 or a material mainly containing SiO_2.

4. The boundary acoustic wave device according to any one of Claims 1 to 3, wherein the first medium is made of $LiNbO_3$ and has Euler angles $[\phi, \theta, \psi]$ satisfying the relationships $-25° < \phi < 25°$, $92° < \theta < 114°$, and $-60° < \psi < 60°$.

5. The boundary acoustic wave device according to any one of Claims 1 to 3, wherein the first medium is made of $LiNbO_3$, and has Euler angles $[\phi, \theta, \psi]$ satisfying the relationships $-25° < \phi < 25°$, $92° < \theta < 114°$, and $60° < \psi < 120°$.

6. The boundary acoustic wave device according to any one of Claims 1 to 3, wherein the first medium is made of $LiNbO_3$ and has Euler angles $[\phi, \theta, \psi]$ satisfying the relationships $-32° < \phi < 32°$, $15° < \theta < 41°$, and $-35° < \psi < 35$.

7. The boundary acoustic wave device according to any one of Claims 1 to 6, wherein the IDT is made of a metal selected from the group consisting of Pt, Au, Cu, Ag, Ni, Ti, Fe, W, Ta, and alloys mainly containing those metals.

8. The boundary acoustic wave device according to any one of Claims 1 to 6, wherein the IDT has a structure formed by alternately disposing a first metal layer having a relatively high density and a second metal layer having a relatively low density.

9. The boundary acoustic wave device according to Claim 8, wherein the first metal layer is disposed at the first medium side.

10. The boundary acoustic wave device according to any one of Claims 1 to 9, wherein the first medium and/or the second medium has a multilayer structure including a plurality of medium layers.

FIG. 1

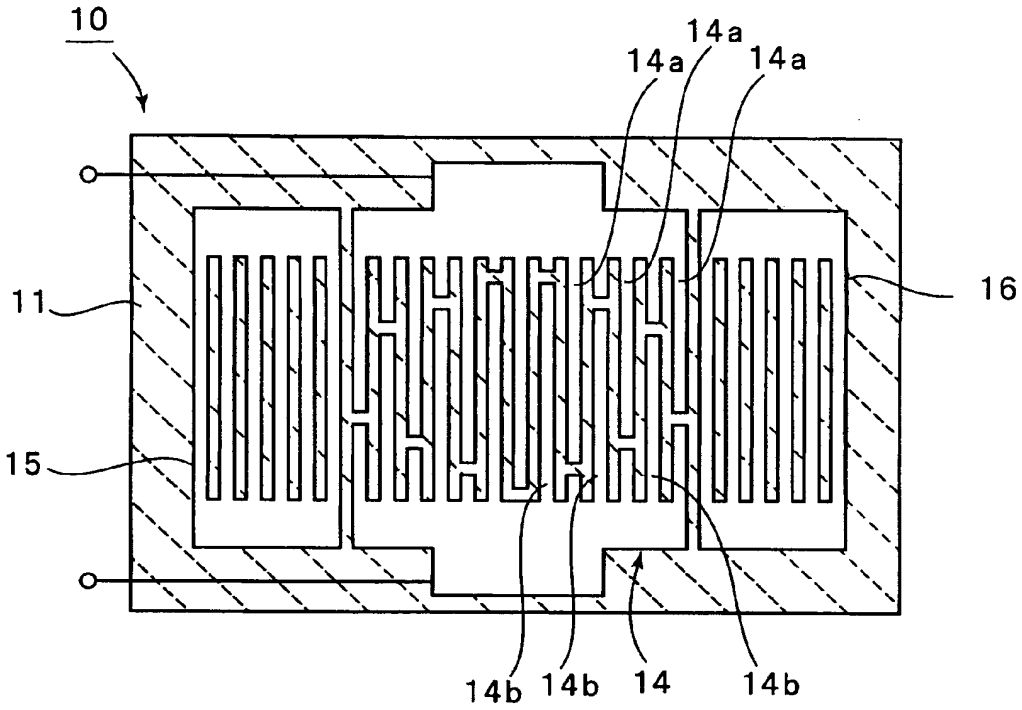
10
14a
14a
14a
11
16
15
14b
14b
14
14b

FIG. 2

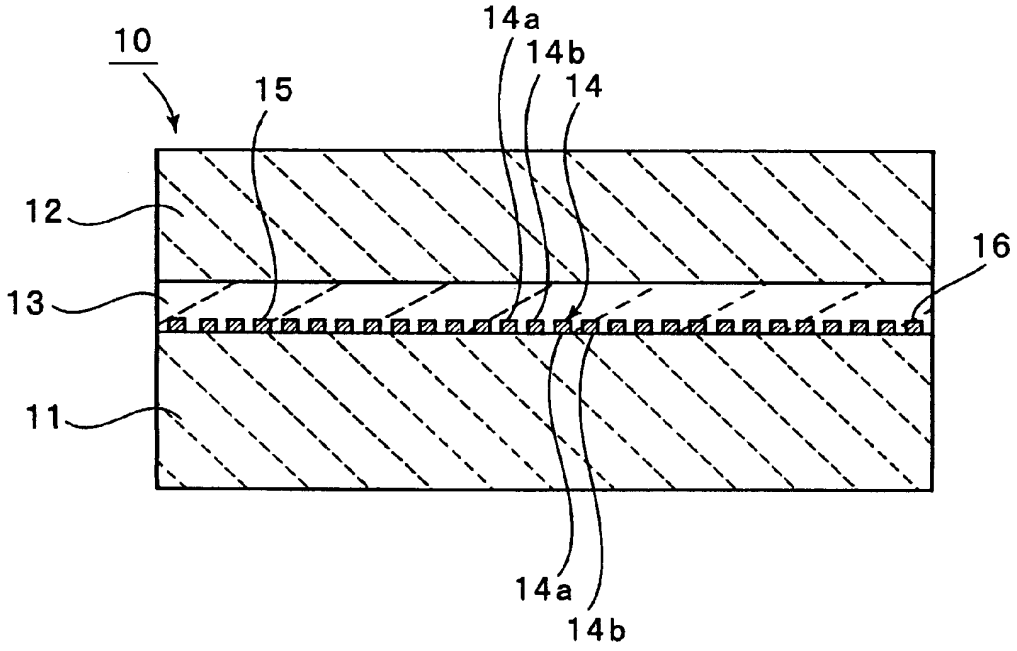
14a
14b
14
10
15
12
16
13
11
14a
14b

FIG. 3

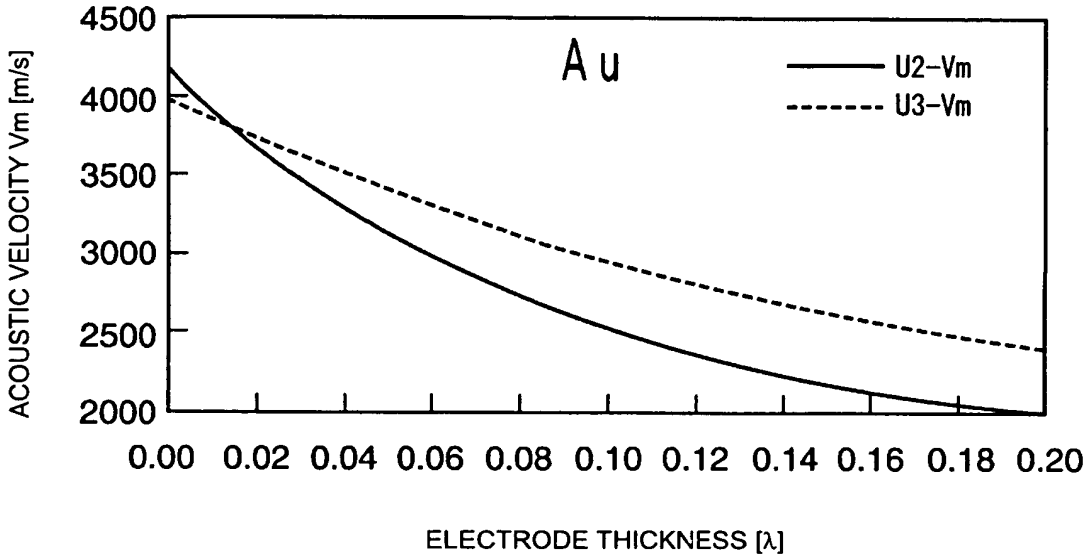
4500
4000
3500
3000
2500
2000
Au
U2-Vm
U3-Vm
ACOUSTIC VELOCITY Vm [m/s]
0.00 0.02 0.04 0.06 0.08 0.10 0.12 0.14 0.16 0.18 0.20
ELECTRODE THICKNESS [λ]

FIG. 4

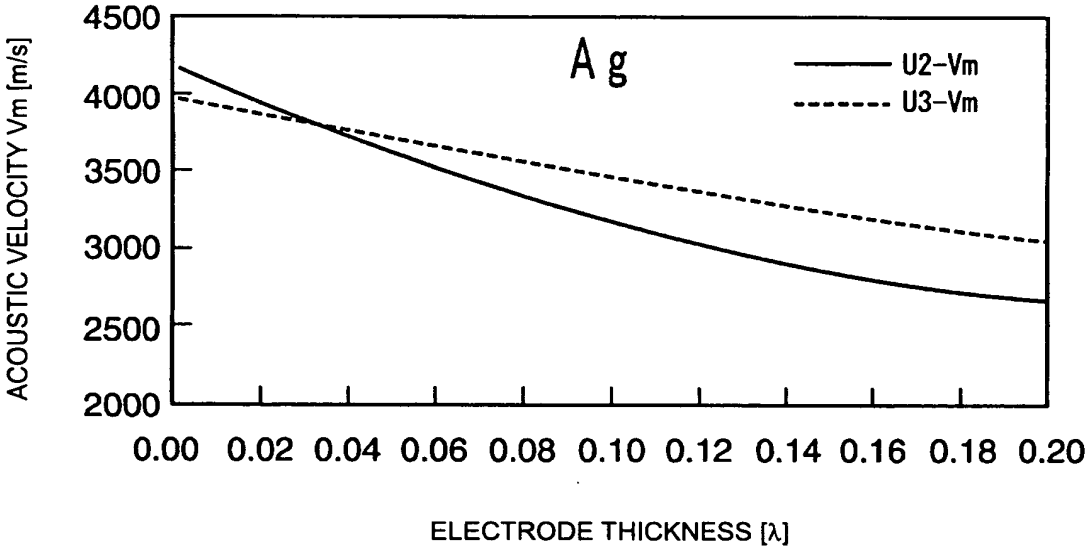
4500
4000
3500
3000
2500
2000
Ag
U2-Vm
U3-Vm
ACOUSTIC VELOCITY Vm [m/s]
0.00 0.02 0.04 0.06 0.08 0.10 0.12 0.14 0.16 0.18 0.20
ELECTRODE THICKNESS [λ]

FIG. 5

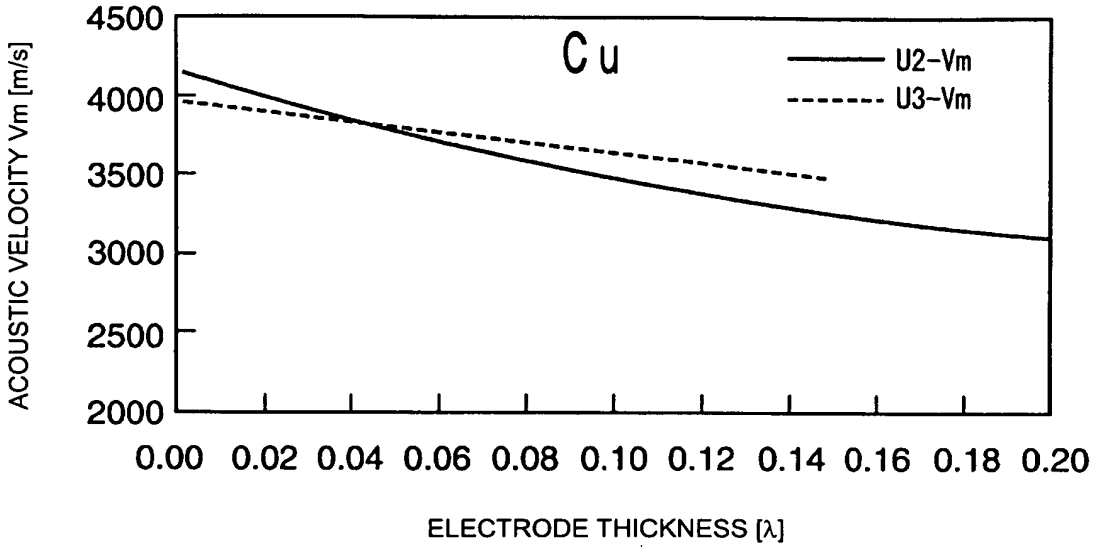
4500
4000
3500
3000
2500
2000
Cu
U2-Vm
U3-Vm
ACOUSTIC VELOCITY Vm [m/s]
0.00 0.02 0.04 0.06 0.08 0.10 0.12 0.14 0.16 0.18 0.20
ELECTRODE THICKNESS [λ]

FIG. 6

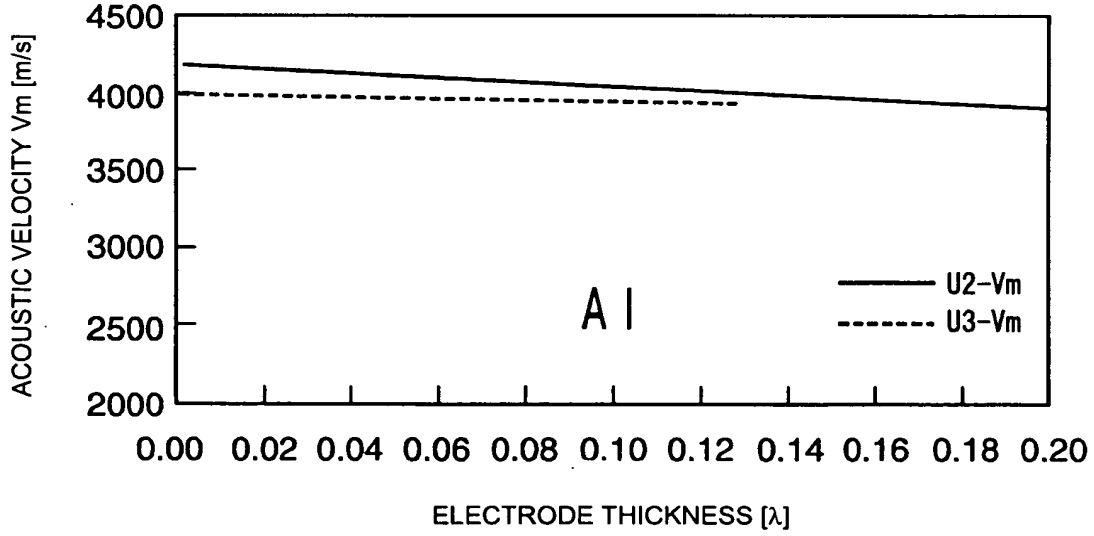
4500
4000
3500
3000
2500
2000
Al
U2-Vm
U3-Vm
ACOUSTIC VELOCITY Vm [m/s]
0.00 0.02 0.04 0.06 0.08 0.10 0.12 0.14 0.16 0.18 0.20
ELECTRODE THICKNESS [λ]

FIG. 7

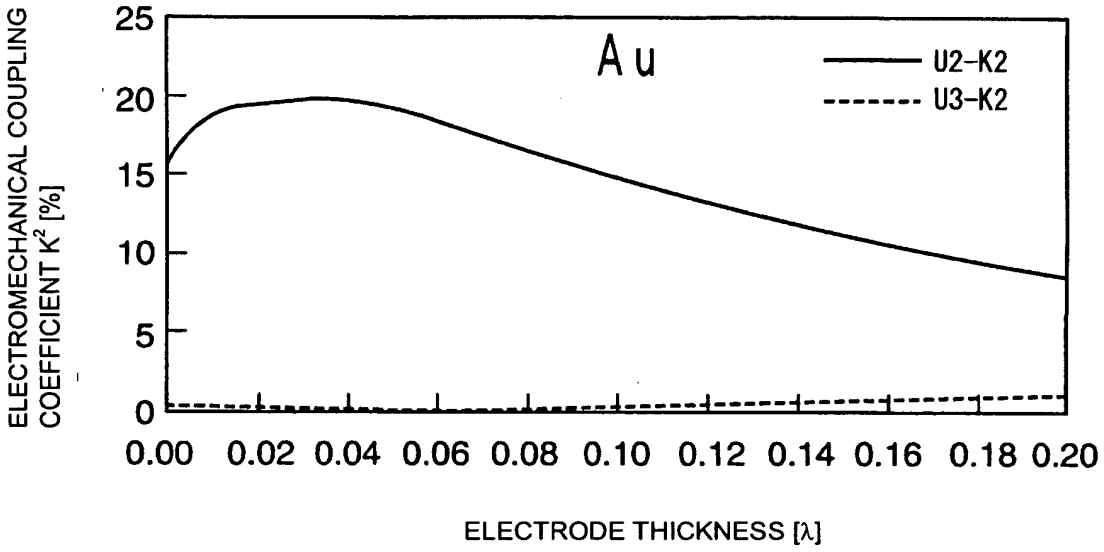
Au
U2-K2
U3-K2
ELECTROMECHANICAL COUPLING COEFFICIENT K² [%]
25
20
15
10
5
0
0.00 0.02 0.04 0.06 0.08 0.10 0.12 0.14 0.16 0.18 0.20
ELECTRODE THICKNESS [λ]

FIG. 8

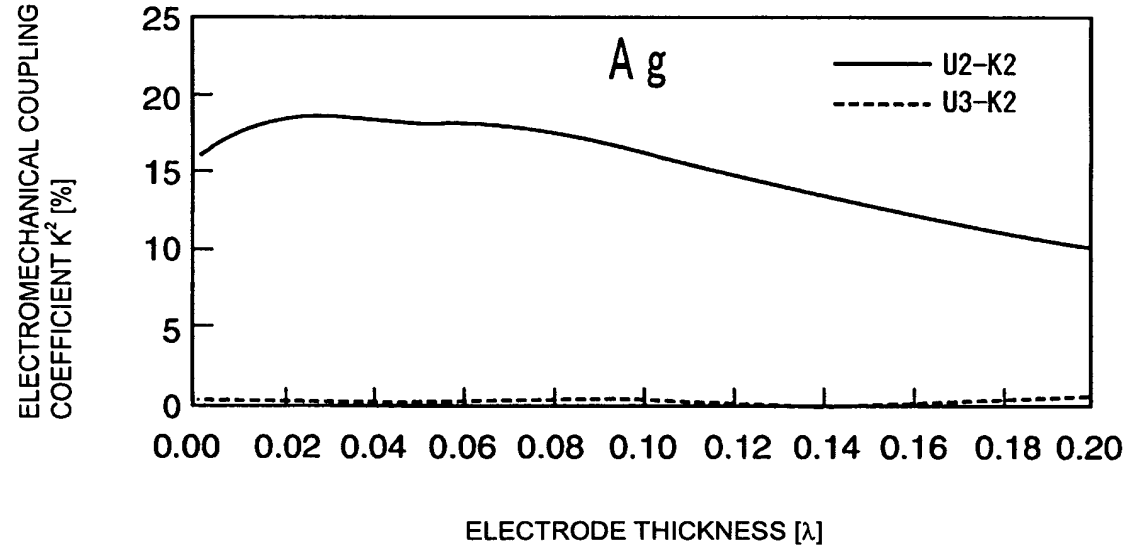
Ag
U2-K2
U3-K2
ELECTROMECHANICAL COUPLING COEFFICIENT K² [%]
25
20
15
10
5
0
0.00 0.02 0.04 0.06 0.08 0.10 0.12 0.14 0.16 0.18 0.20
ELECTRODE THICKNESS [λ]

FIG. 9

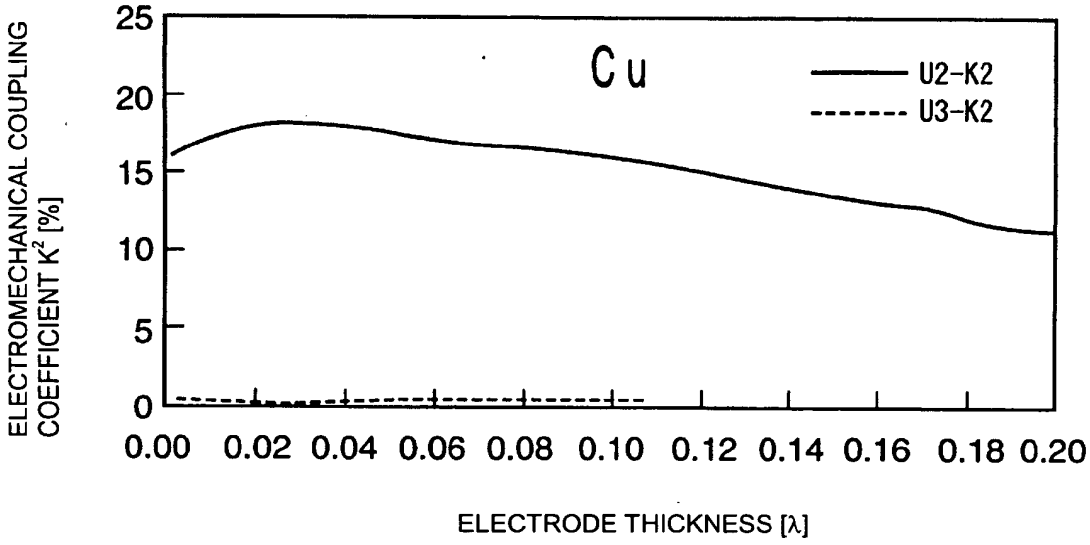
Cu
U2-K2
U3-K2
ELECTROMECHANICAL COUPLING COEFFICIENT K² [%]
25
20
15
10
5
0
0.00 0.02 0.04 0.06 0.08 0.10 0.12 0.14 0.16 0.18 0.20
ELECTRODE THICKNESS [λ]

FIG. 10

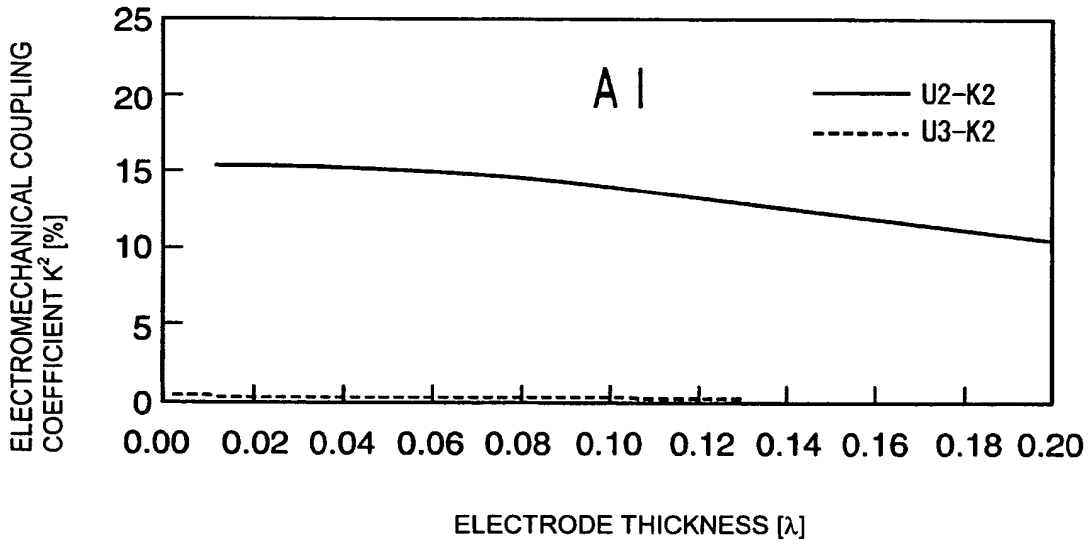
Al
U2-K2
U3-K2
ELECTROMECHANICAL COUPLING COEFFICIENT K² [%]
25
20
15
10
5
0
0.00 0.02 0.04 0.06 0.08 0.10 0.12 0.14 0.16 0.18 0.20
ELECTRODE THICKNESS [λ]

FIG. 11

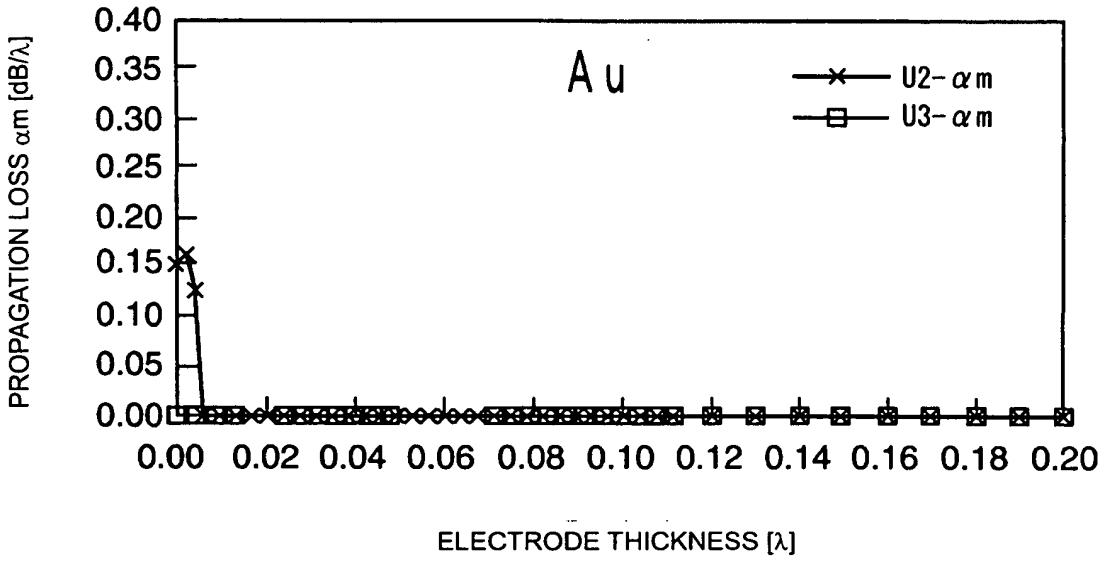
Au
U2-αm
U3-αm
PROPAGATION LOSS αm [dB/λ]
0.40
0.35
0.30
0.25
0.20
0.15
0.10
0.05
0.00
0.00 0.02 0.04 0.06 0.08 0.10 0.12 0.14 0.16 0.18 0.20
ELECTRODE THICKNESS [λ]

FIG. 12

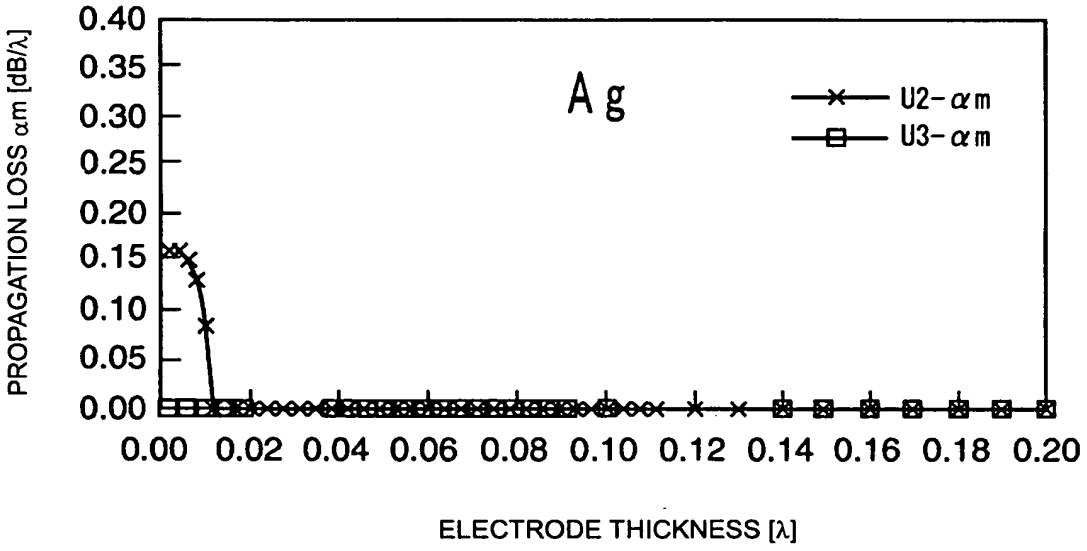
Ag
U2-αm
U3-αm
PROPAGATION LOSS αm [dB/λ]
0.40
0.35
0.30
0.25
0.20
0.15
0.10
0.05
0.00
0.00 0.02 0.04 0.06 0.08 0.10 0.12 0.14 0.16 0.18 0.20
ELECTRODE THICKNESS [λ]

FIG. 13

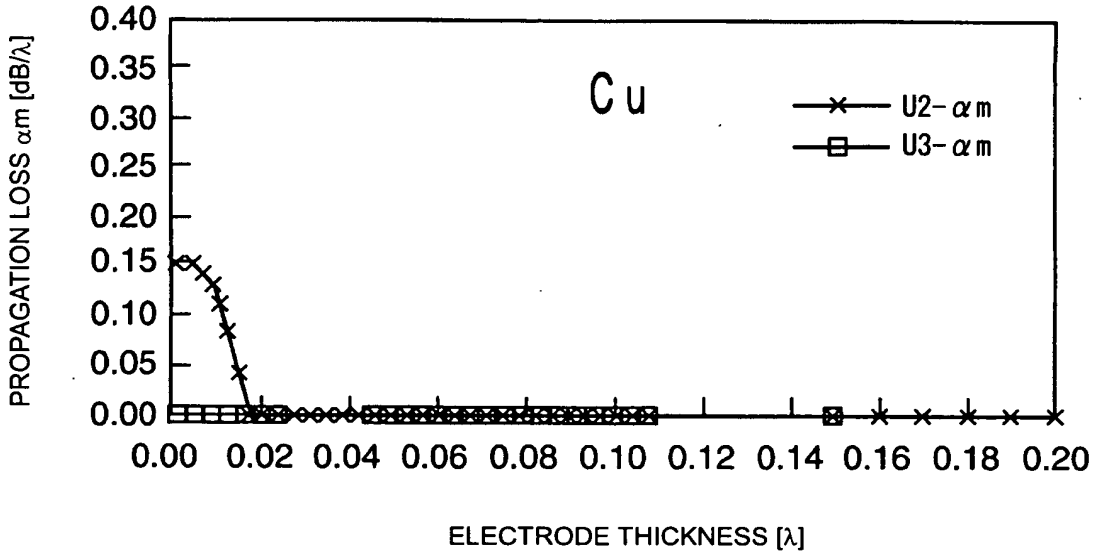
PROPAGATION LOSS αm [dB/λ]
0.40
0.35
0.30
0.25
0.20
0.15
0.10
0.05
0.00
Cu
U2-αm
U3-αm
0.00 0.02 0.04 0.06 0.08 0.10 0.12 0.14 0.16 0.18 0.20
ELECTRODE THICKNESS [λ]

FIG. 14

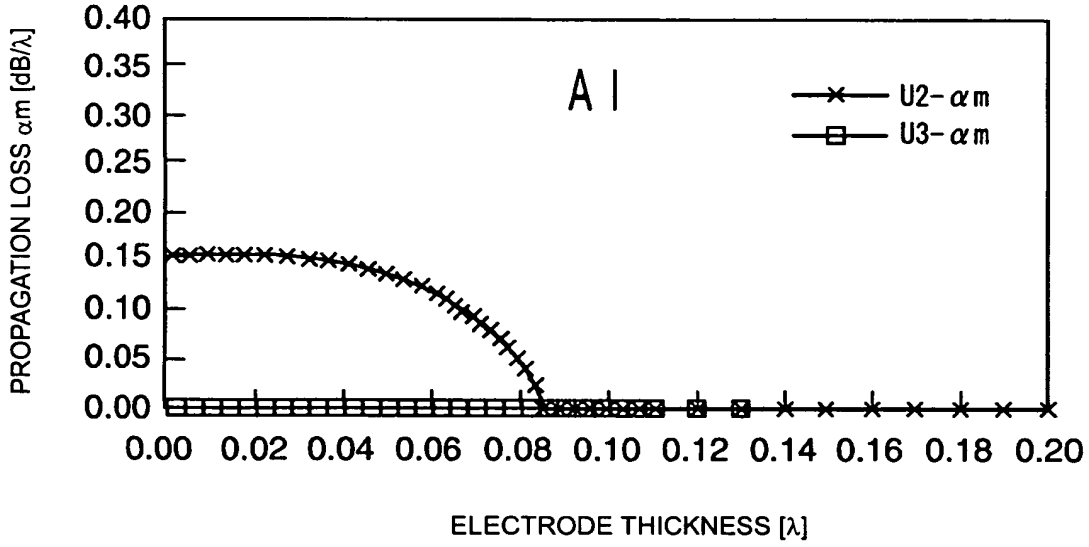
PROPAGATION LOSS αm [dB/λ]
0.40
0.35
0.30
0.25
0.20
0.15
0.10
0.05
0.00
Al
U2-αm
U3-αm
0.00 0.02 0.04 0.06 0.08 0.10 0.12 0.14 0.16 0.18 0.20
ELECTRODE THICKNESS [λ]

FIG. 15

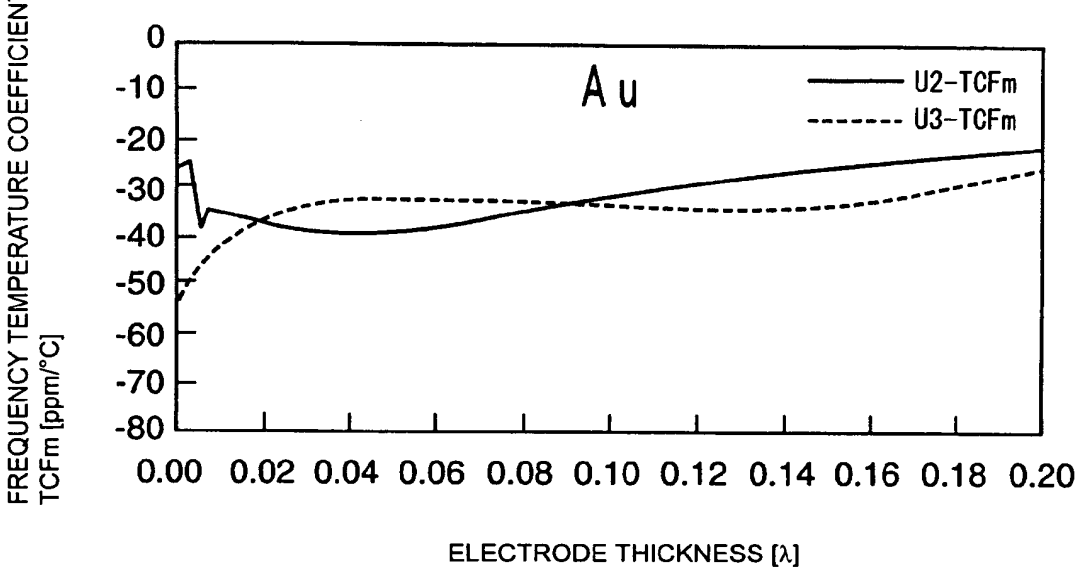
FREQUENCY TEMPERATURE COEFFICIENT
TCFm [ppm/°C]
0
-10
-20
-30
-40
-50
-60
-70
-80
Au
U2-TCFm
U3-TCFm
0.00 0.02 0.04 0.06 0.08 0.10 0.12 0.14 0.16 0.18 0.20
ELECTRODE THICKNESS [λ]

FIG. 16

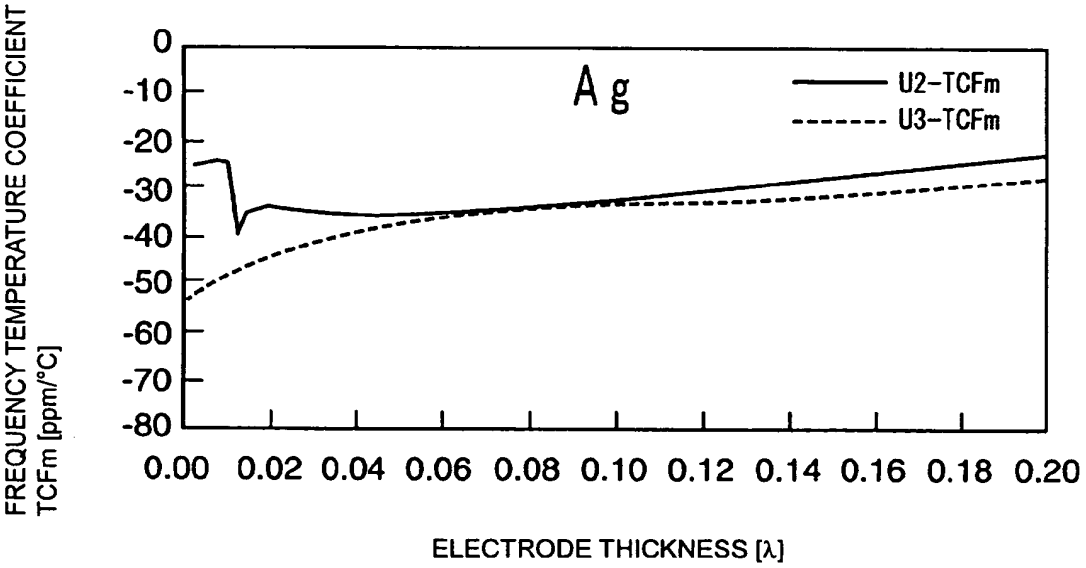
FREQUENCY TEMPERATURE COEFFICIENT
TCFm [ppm/°C]
0
-10
-20
-30
-40
-50
-60
-70
-80
Ag
U2-TCFm
U3-TCFm
0.00 0.02 0.04 0.06 0.08 0.10 0.12 0.14 0.16 0.18 0.20
ELECTRODE THICKNESS [λ]

FIG. 17

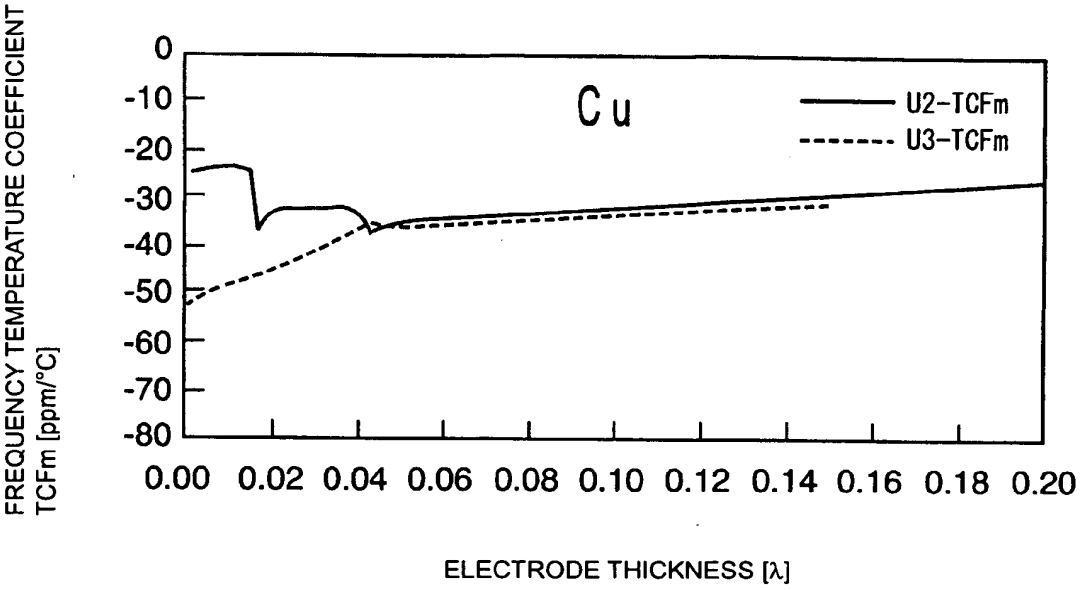
FREQUENCY TEMPERATURE COEFFICIENT
TCFm [ppm/°C]
0
-10
-20
-30
-40
-50
-60
-70
-80
Cu
U2-TCFm
U3-TCFm
0.00 0.02 0.04 0.06 0.08 0.10 0.12 0.14 0.16 0.18 0.20
ELECTRODE THICKNESS [λ]

FIG. 18

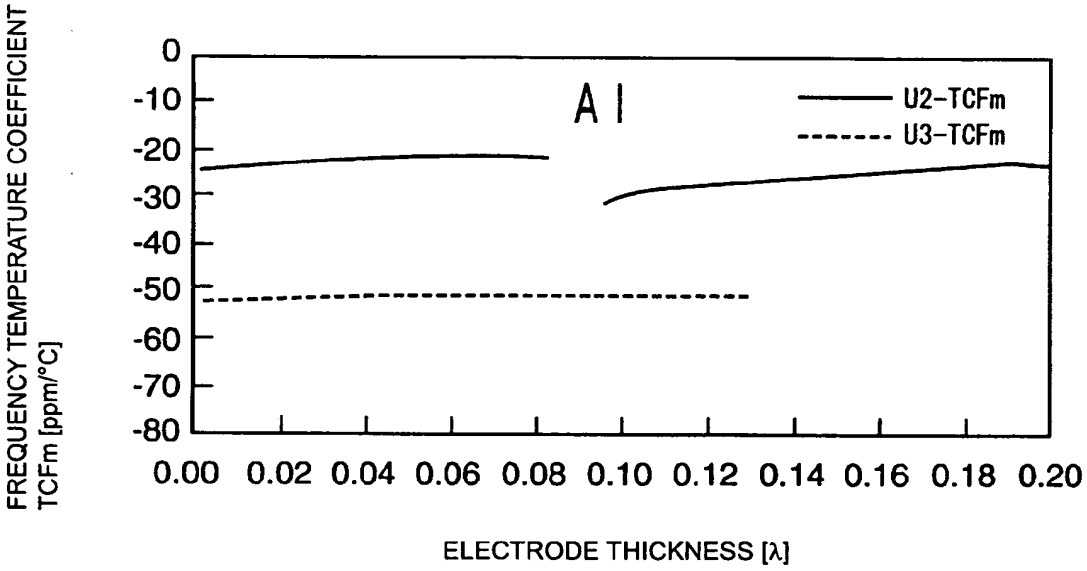
FREQUENCY TEMPERATURE COEFFICIENT
TCFm [ppm/°C]
0
-10
-20
-30
-40
-50
-60
-70
-80
Al
U2-TCFm
U3-TCFm
0.00 0.02 0.04 0.06 0.08 0.10 0.12 0.14 0.16 0.18 0.20
ELECTRODE THICKNESS [λ]

FIG. 19

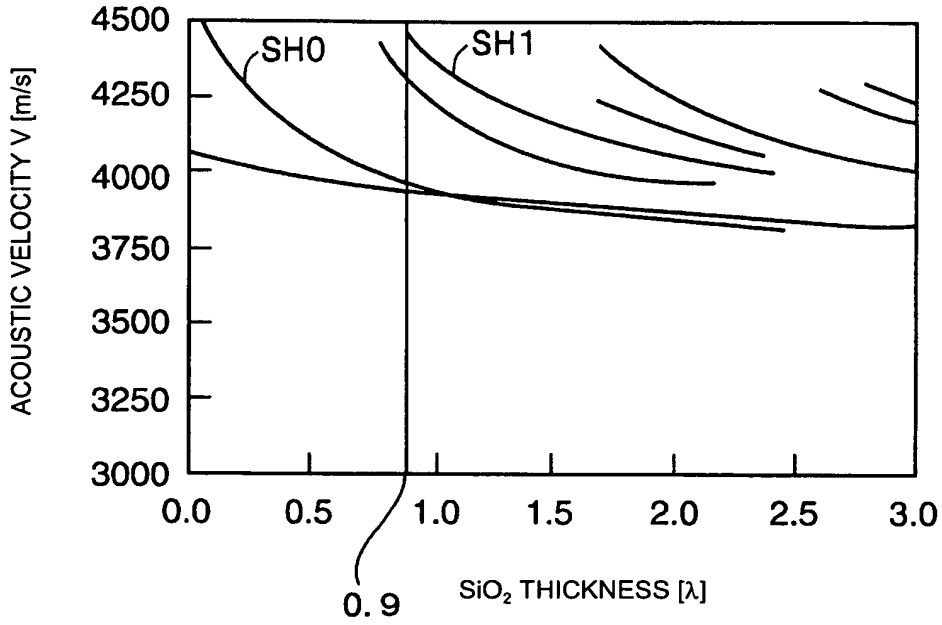
4500
4250
4000
3750
3500
3250
3000
ACOUSTIC VELOCITY V [m/s]
SH0
SH1
0.0
0.5
1.0
1.5
2.0
2.5
3.0
0.9
SiO2 THICKNESS [λ]

FIG. 20

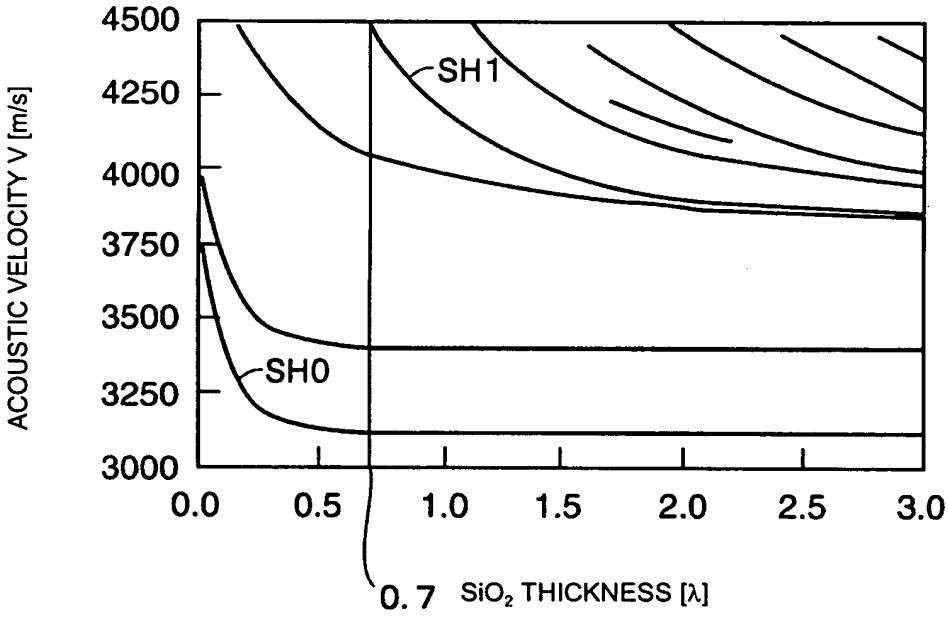
4500
4250
4000
3750
3500
3250
3000
ACOUSTIC VELOCITY V [m/s]
SH1
SH0
0.0
0.5
1.0
1.5
2.0
2.5
3.0
0.7
SiO2 THICKNESS [λ]

FIG. 21

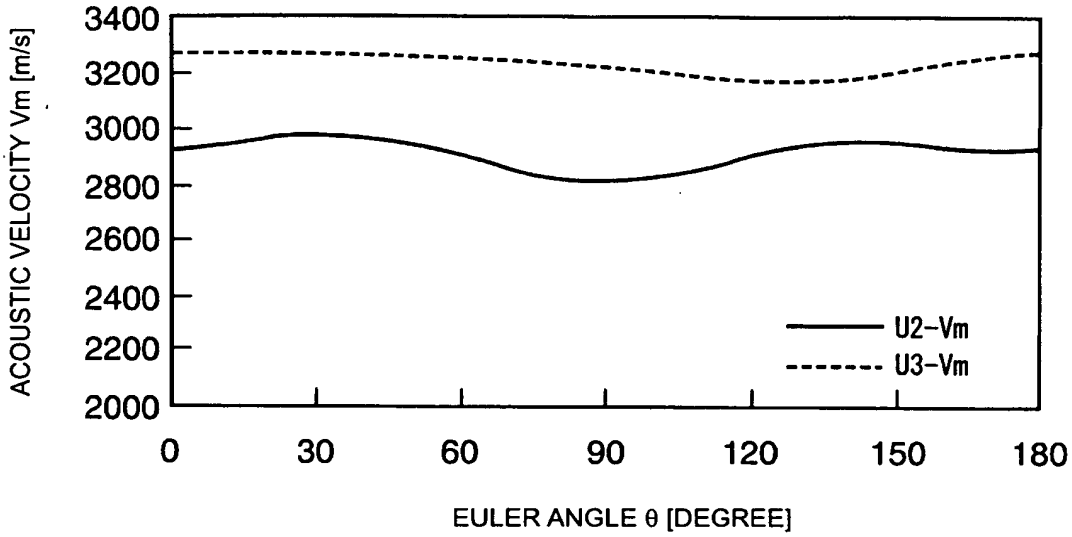
ACOUSTIC VELOCITY Vm [m/s]
3400
3200
3000
2800
2600
2400
2200
2000
0
30
60
90
120
150
180
U2-Vm
U3-Vm
EULER ANGLE θ [DEGREE]

FIG. 22

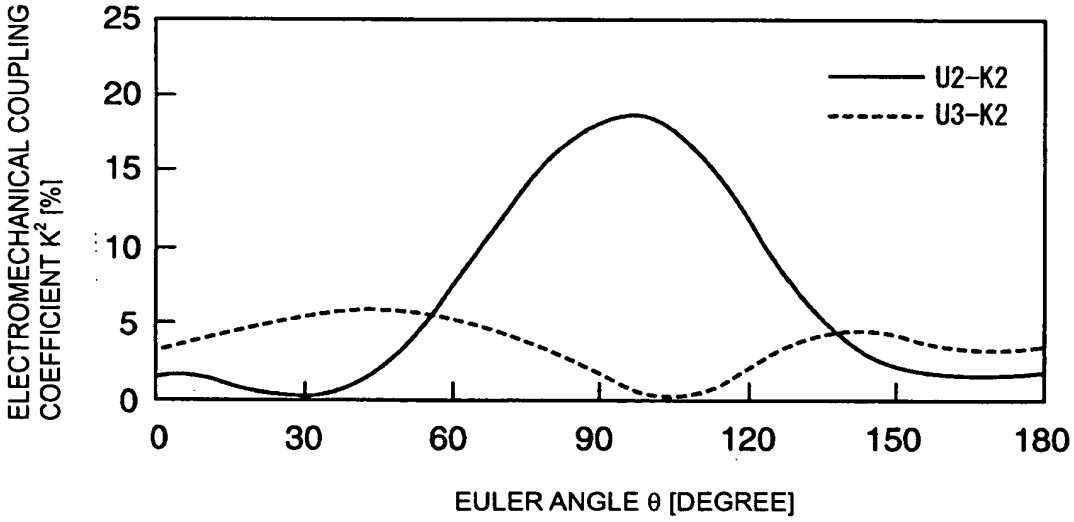
ELECTROMECHANICAL COUPLING COEFFICIENT K² [%]
25
20
15
10
5
0
0
30
60
90
120
150
180
U2-K2
U3-K2
EULER ANGLE θ [DEGREE]

FIG. 23

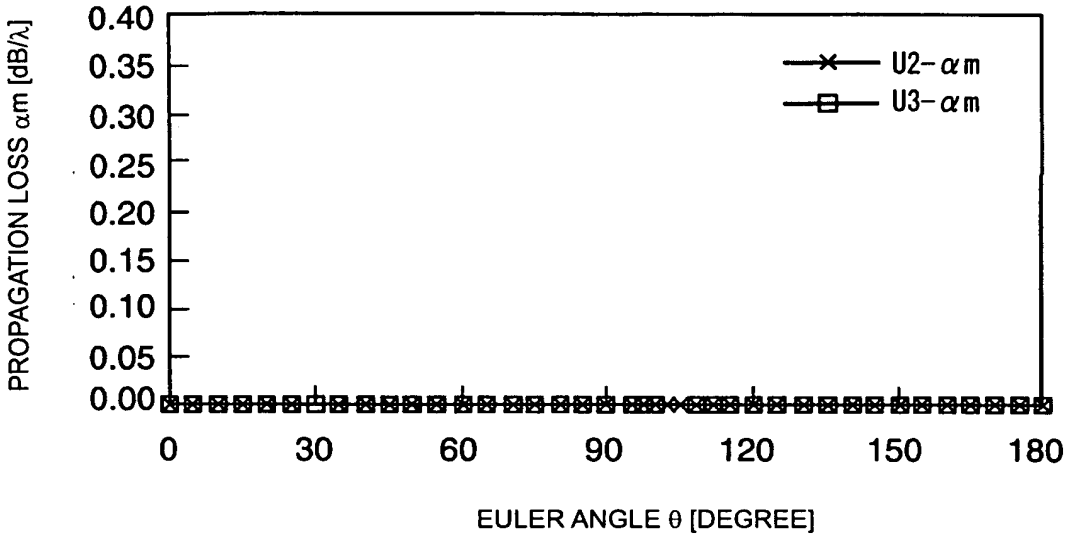
PROPAGATION LOSS αm [dB/λ]
0.40
0.35
0.30
0.25
0.20
0.15
0.10
0.05
0.00
U2-αm
U3-αm
0
30
60
90
120
150
180
EULER ANGLE θ [DEGREE]

FIG. 24

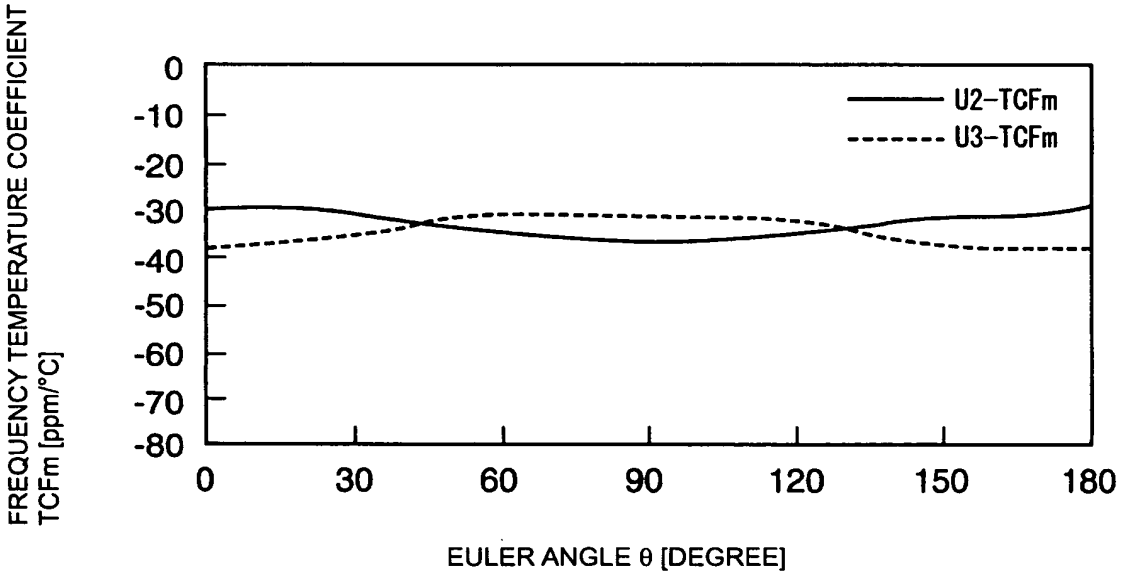
FREQUENCY TEMPERATURE COEFFICIENT TCFm [ppm/°C]
0
-10
-20
-30
-40
-50
-60
-70
-80
U2-TCFm
U3-TCFm
0
30
60
90
120
150
180
EULER ANGLE θ [DEGREE]

FIG. 25

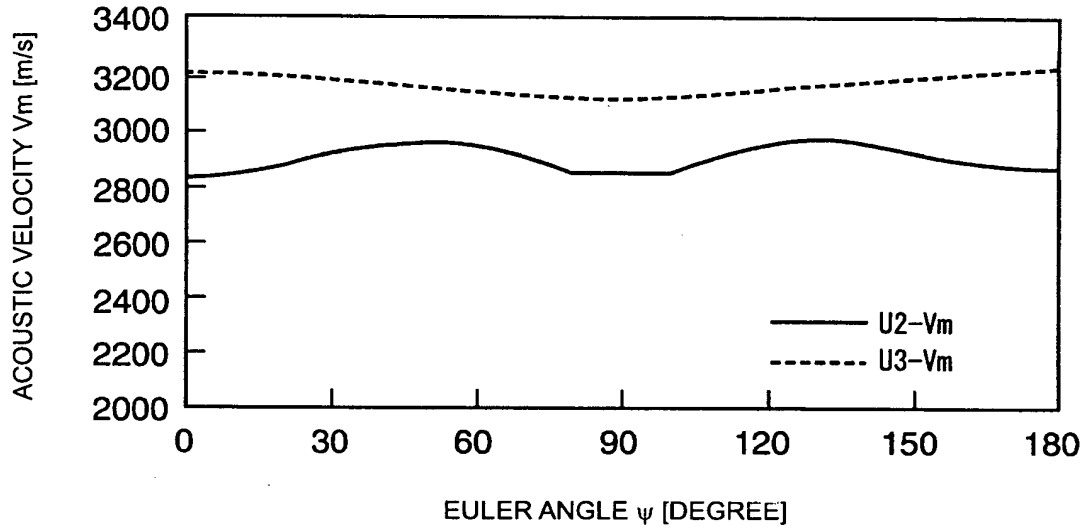
ACOUSTIC VELOCITY Vm [m/s]
3400
3200
3000
2800
2600
2400
2200
2000
0
30
60
90
120
150
180
U2-Vm
U3-Vm
EULER ANGLE ψ [DEGREE]

FIG. 26

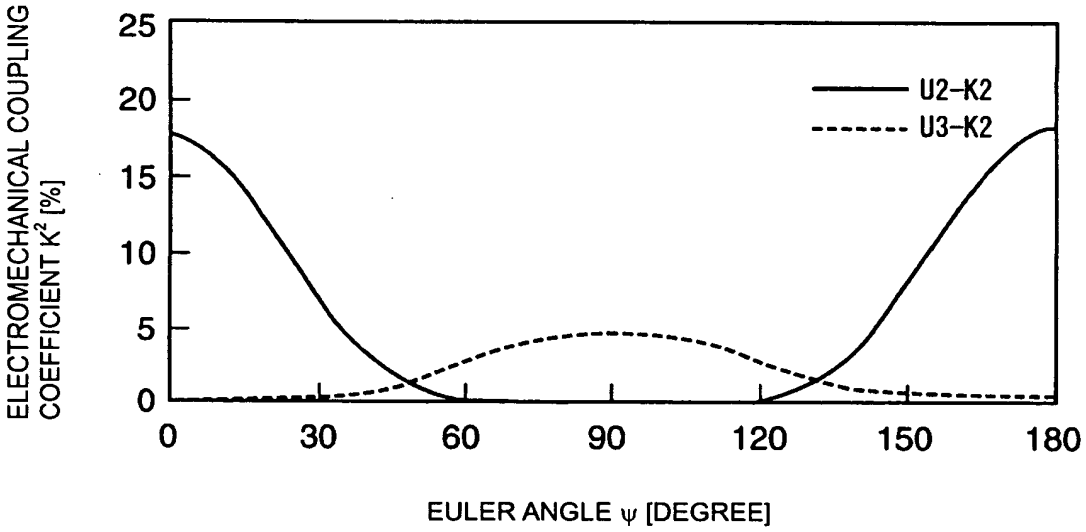
ELECTROMECHANICAL COUPLING COEFFICIENT K² [%]
25
20
15
10
5
0
0
30
60
90
120
150
180
U2-K2
U3-K2
EULER ANGLE ψ [DEGREE]

FIG. 27

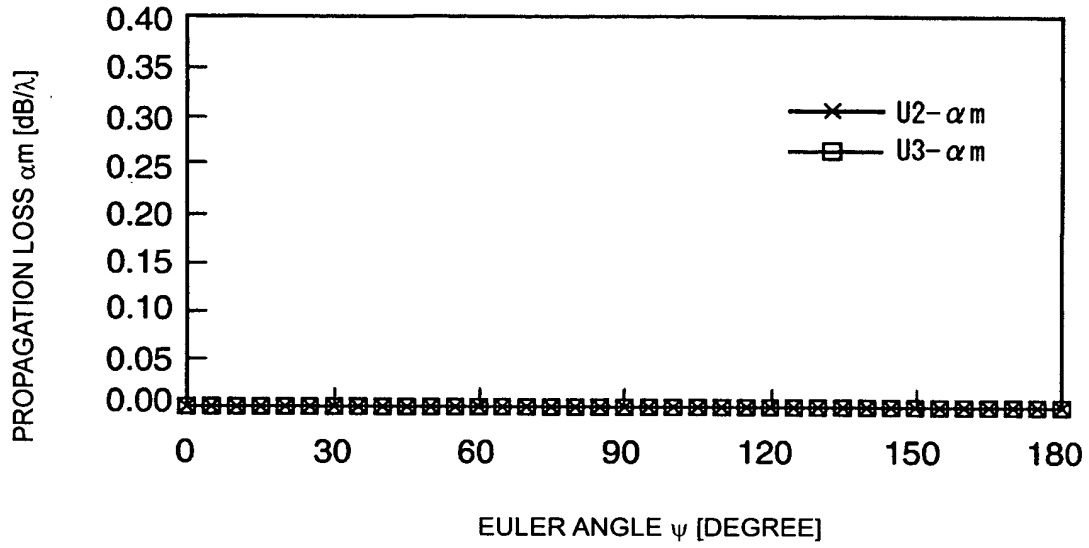
0.40
0.35
0.30
0.25
0.20
0.15
0.10
0.05
0.00
PROPAGATION LOSS αm [dB/λ]
U2-αm
U3-αm
0
30
60
90
120
150
180
EULER ANGLE ψ [DEGREE]

FIG. 28

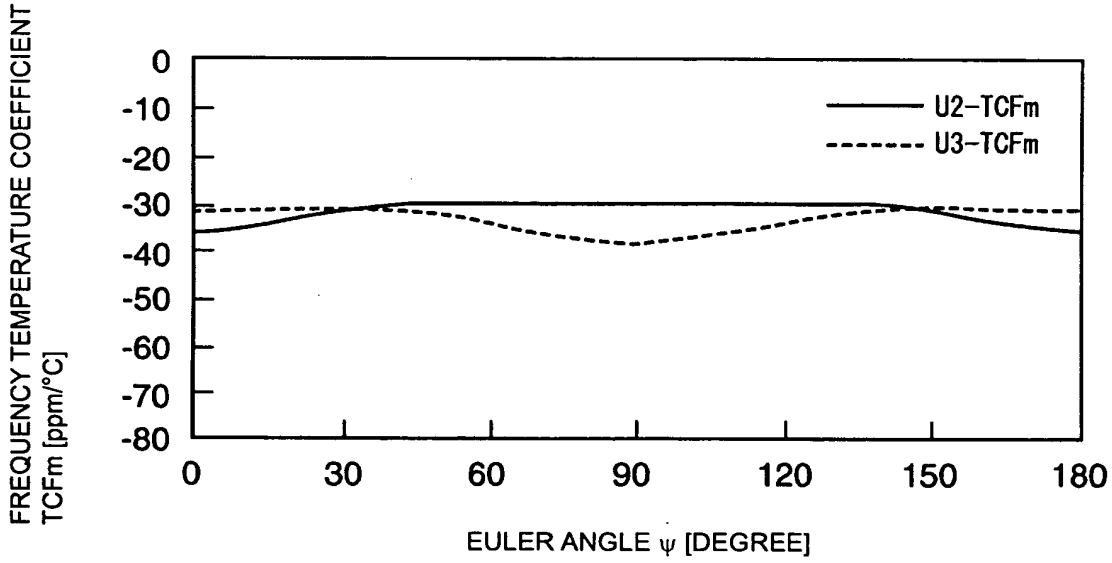
0
-10
-20
-30
-40
-50
-60
-70
-80
FREQUENCY TEMPERATURE COEFFICIENT TCFm [ppm/°C]
U2-TCFm
U3-TCFm
0
30
60
90
120
150
180
EULER ANGLE ψ [DEGREE]

FIG. 29

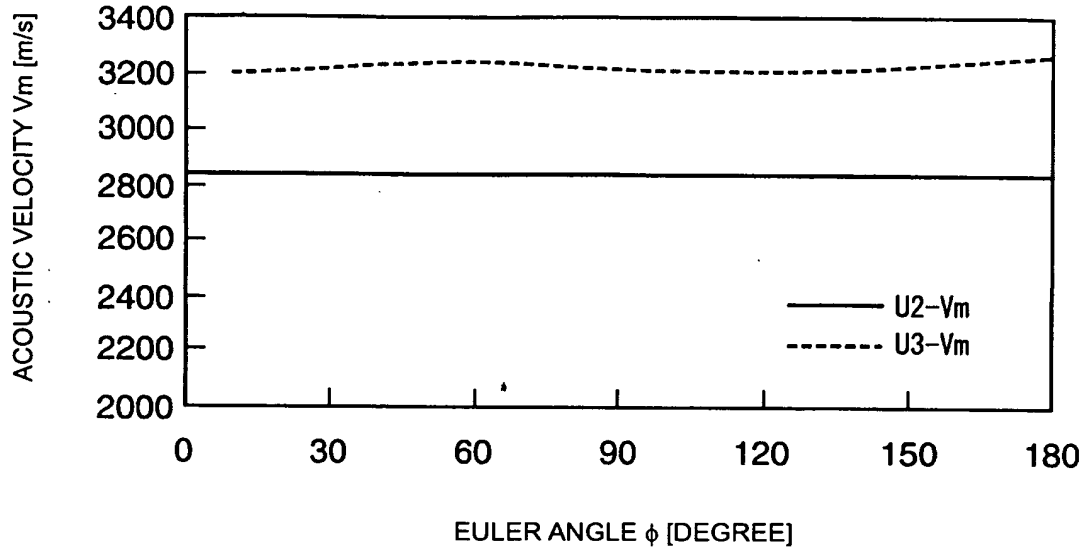
ACOUSTIC VELOCITY Vm [m/s]
3400
3200
3000
2800
2600
2400
2200
2000
0
30
60
90
120
150
180
U2-Vm
U3-Vm
EULER ANGLE ϕ [DEGREE]

FIG. 30

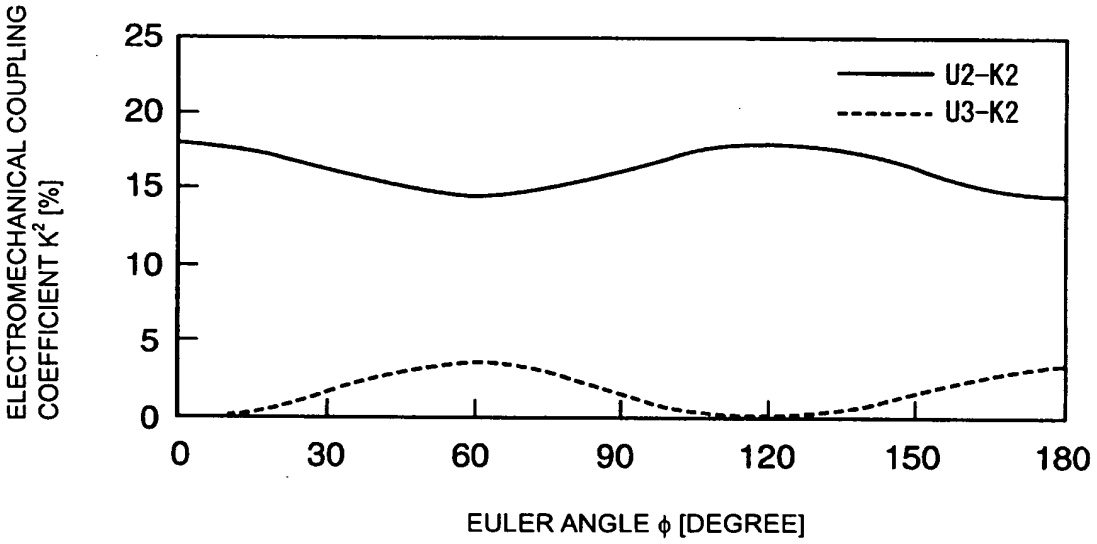
ELECTROMECHANICAL COUPLING COEFFICIENT K² [%]
25
20
15
10
5
0
0
30
60
90
120
150
180
U2-K2
U3-K2
EULER ANGLE ϕ [DEGREE]

FIG. 31

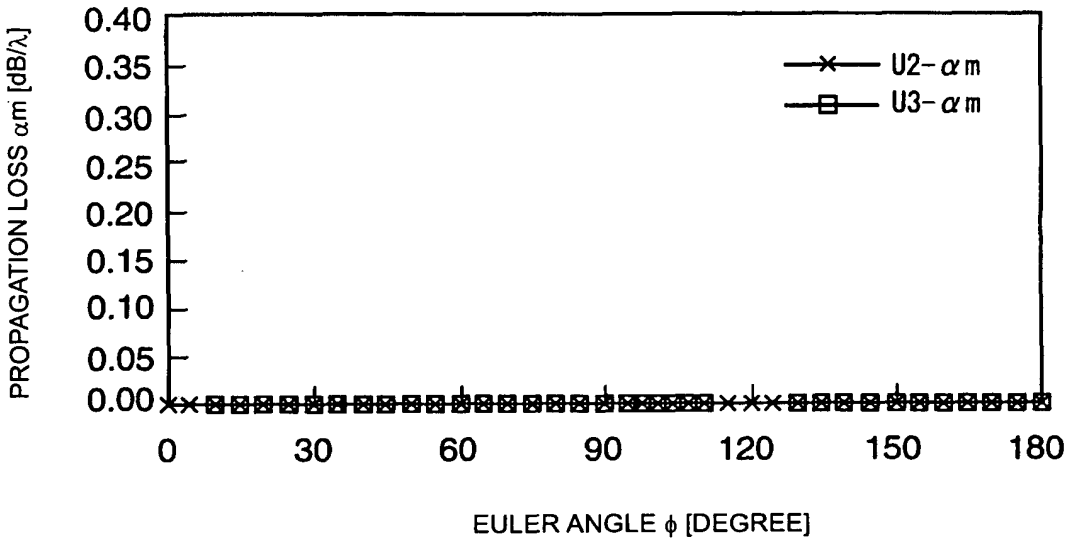
PROPAGATION LOSS αm [dB/λ]
0.40
0.35
0.30
0.25
0.20
0.15
0.10
0.05
0.00
U2-αm
U3-αm
0
30
60
90
120
150
180
EULER ANGLE ϕ [DEGREE]

FIG. 32

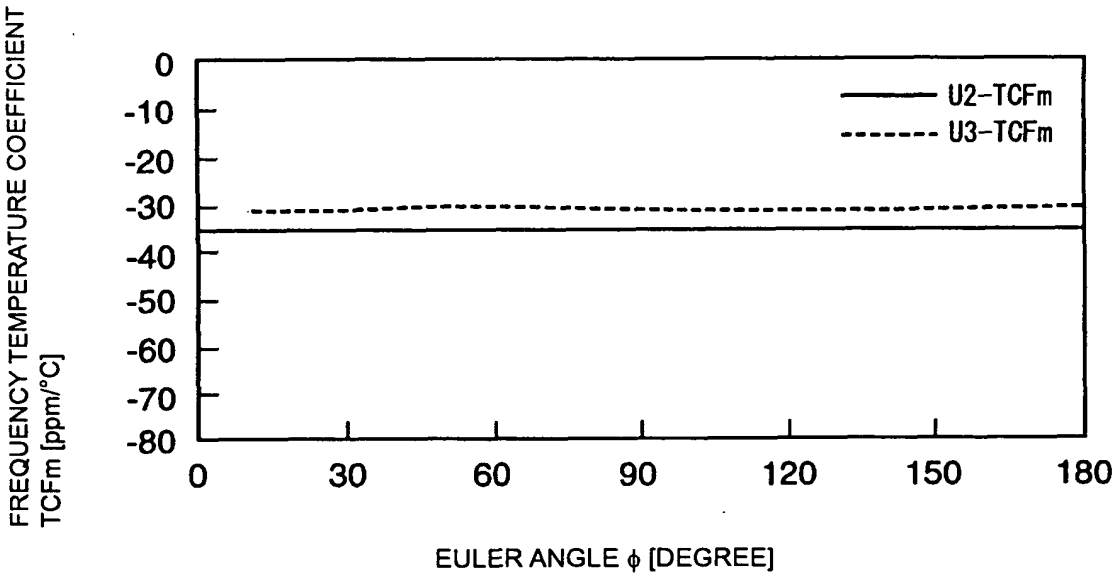
FREQUENCY TEMPERATURE COEFFICIENT
TCFm [ppm/°C]
0
-10
-20
-30
-40
-50
-60
-70
-80
U2-TCFm
U3-TCFm
0
30
60
90
120
150
180
EULER ANGLE ϕ [DEGREE]

FIG. 33

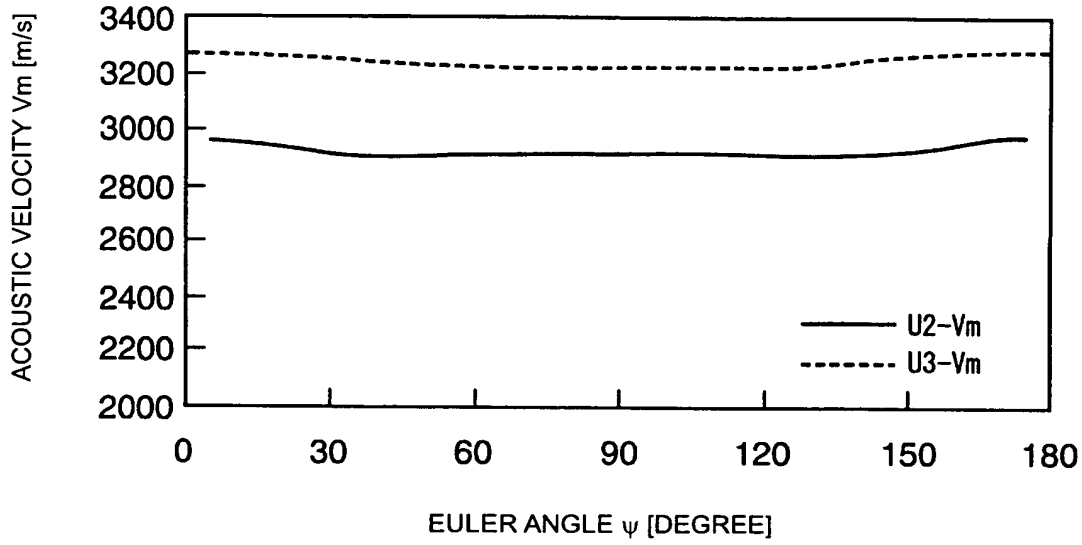
ACOUSTIC VELOCITY Vm [m/s]
3400
3200
3000
2800
2600
2400
2200
2000
0
30
60
90
120
150
180
U2-Vm
U3-Vm
EULER ANGLE ψ [DEGREE]

FIG. 34

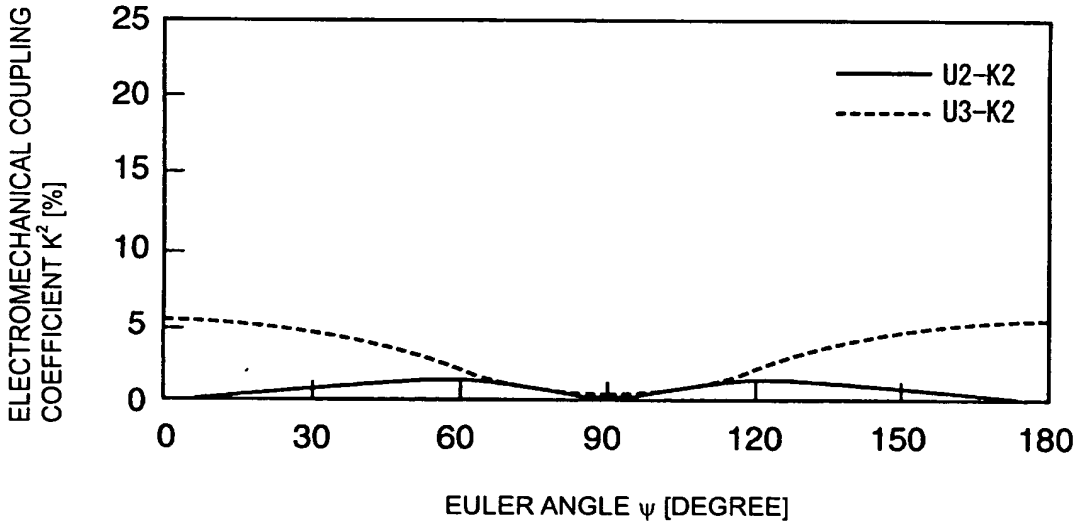
ELECTROMECHANICAL COUPLING COEFFICIENT K² [%]
25
20
15
10
5
0
0
30
60
90
120
150
180
U2-K2
U3-K2
EULER ANGLE ψ [DEGREE]

FIG. 35

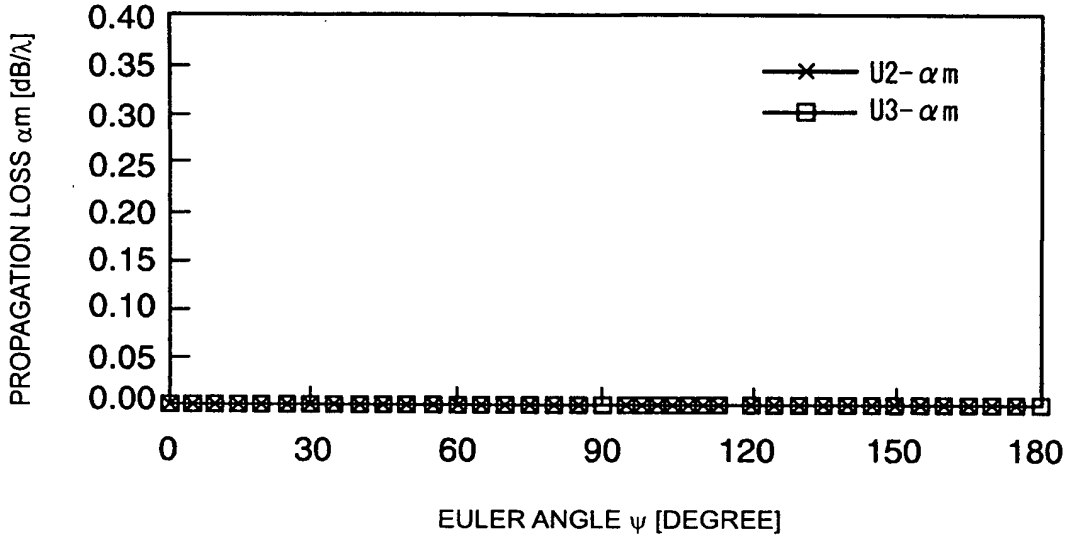
PROPAGATION LOSS αm [dB/λ]
0.40
0.35
0.30
0.25
0.20
0.15
0.10
0.05
0.00
U2-αm
U3-αm
0
30
60
90
120
150
180
EULER ANGLE ψ [DEGREE]

FIG. 36

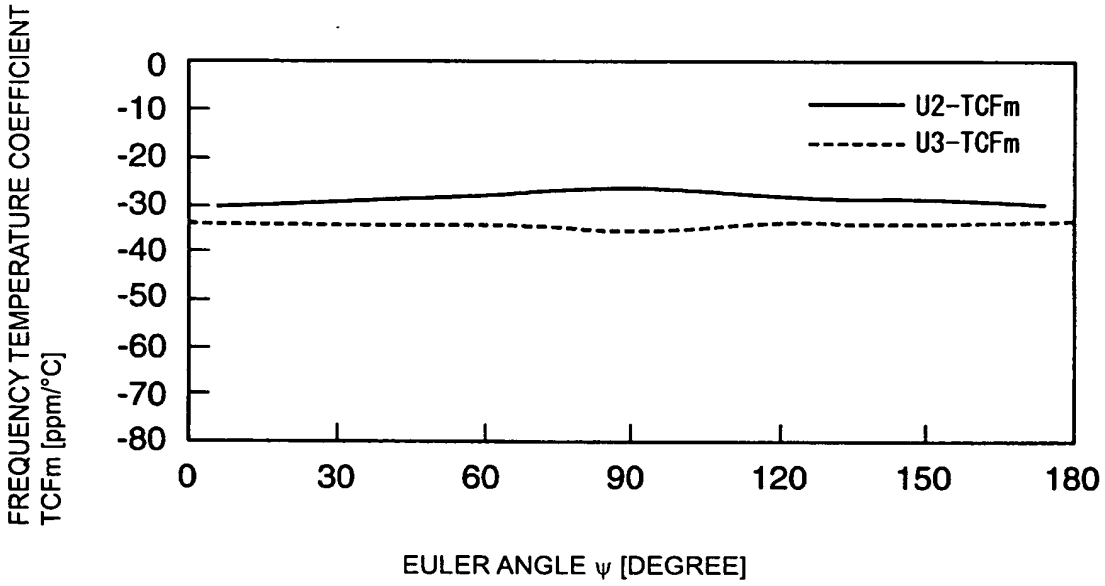
FREQUENCY TEMPERATURE COEFFICIENT
TCFm [ppm/°C]
0
-10
-20
-30
-40
-50
-60
-70
-80
U2-TCFm
U3-TCFm
0
30
60
90
120
150
180
EULER ANGLE ψ [DEGREE]

FIG. 37

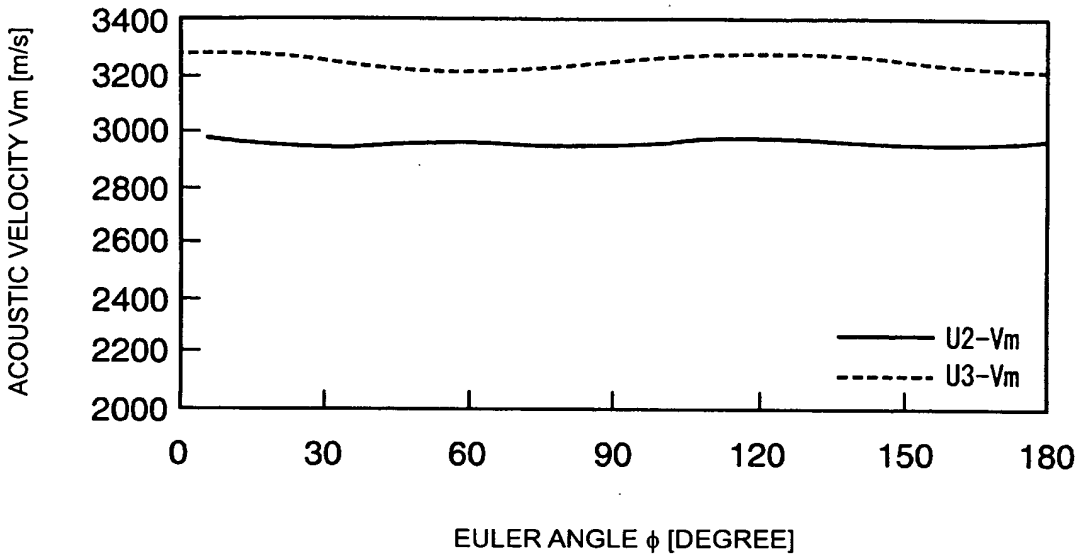
ACOUSTIC VELOCITY Vm [m/s]
3400
3200
3000
2800
2600
2400
2200
2000
0
30
60
90
120
150
180
U2-Vm
U3-Vm
EULER ANGLE ϕ [DEGREE]

FIG. 38

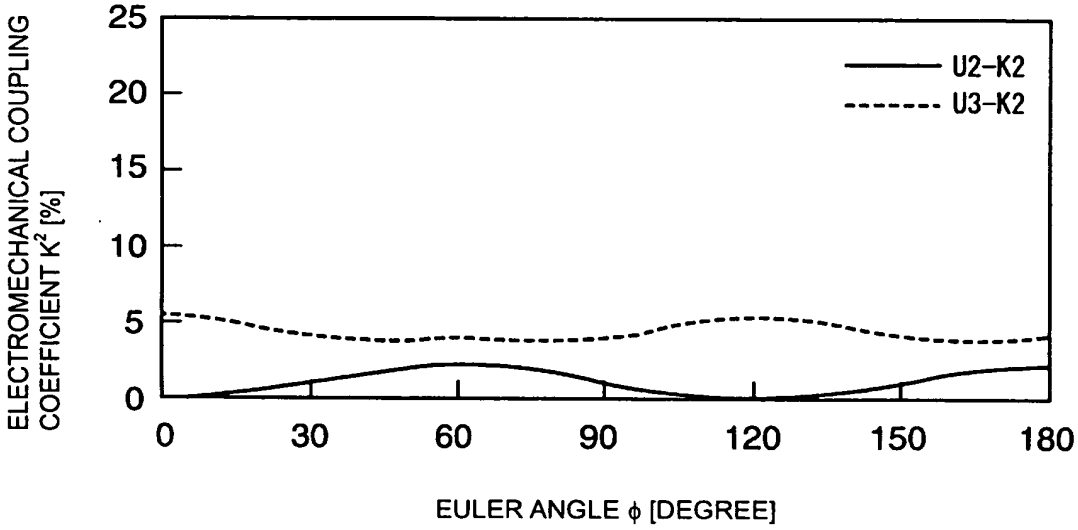
ELECTROMECHANICAL COUPLING COEFFICIENT K² [%]
25
20
15
10
5
0
0
30
60
90
120
150
180
U2-K2
U3-K2
EULER ANGLE ϕ [DEGREE]

FIG. 39

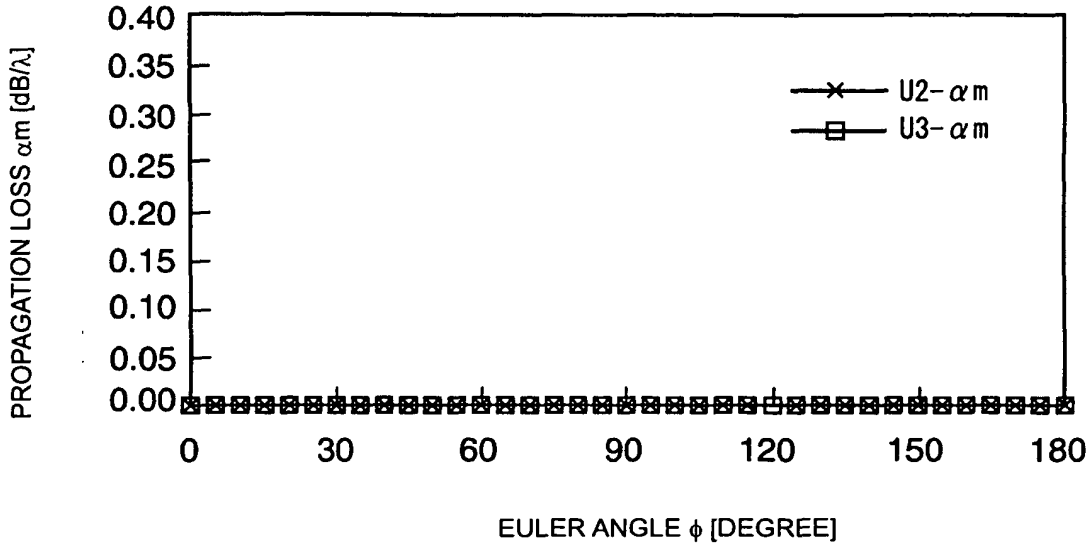
PROPAGATION LOSS αm [dB/λ]
0.40
0.35
0.30
0.25
0.20
0.15
0.10
0.05
0.00
U2-αm
U3-αm
0
30
60
90
120
150
180
EULER ANGLE ϕ [DEGREE]

FIG. 40

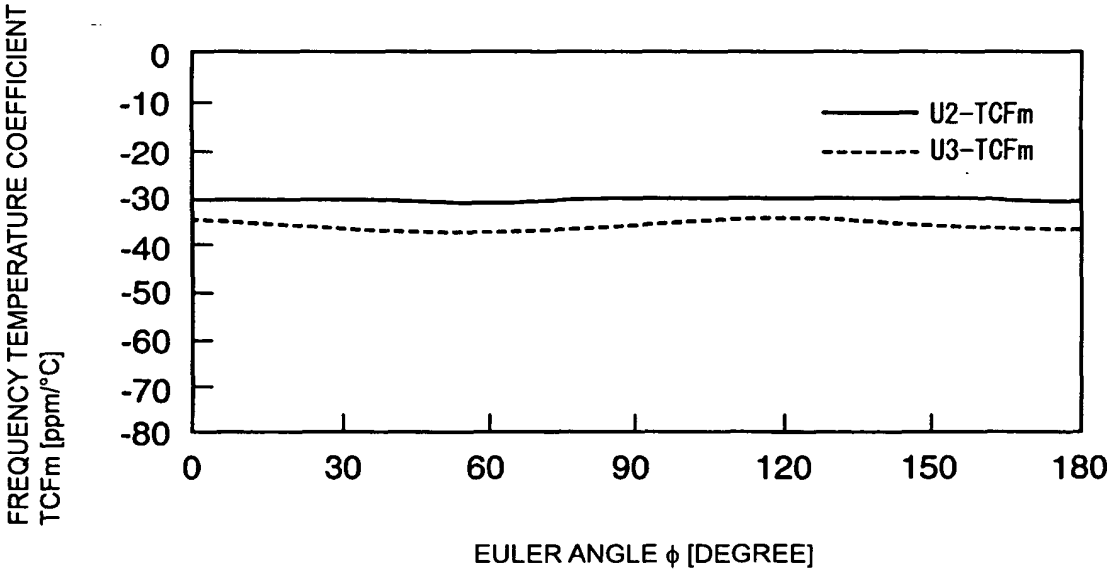
FREQUENCY TEMPERATURE COEFFICIENT
TCFm [ppm/°C]
0
-10
-20
-30
-40
-50
-60
-70
-80
U2-TCFm
U3-TCFm
0
30
60
90
120
150
180
EULER ANGLE ϕ [DEGREE]

FIG. 41

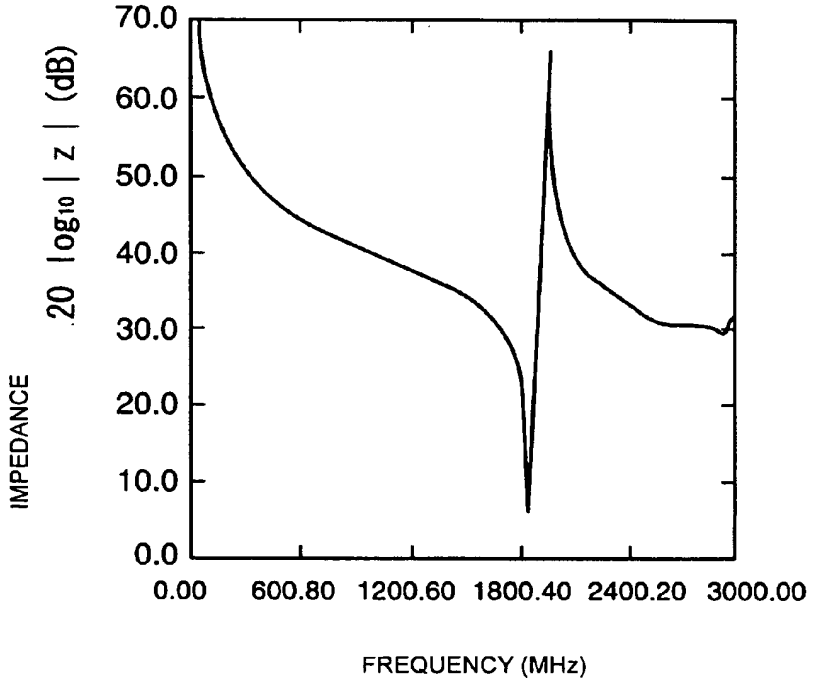
70.0
60.0
50.0
40.0
30.0
20.0
10.0
0.0
20 log10 | z | (dB)
IMPEDANCE
0.00
600.80
1200.60
1800.40
2400.20
3000.00
FREQUENCY (MHz)

FIG. 42

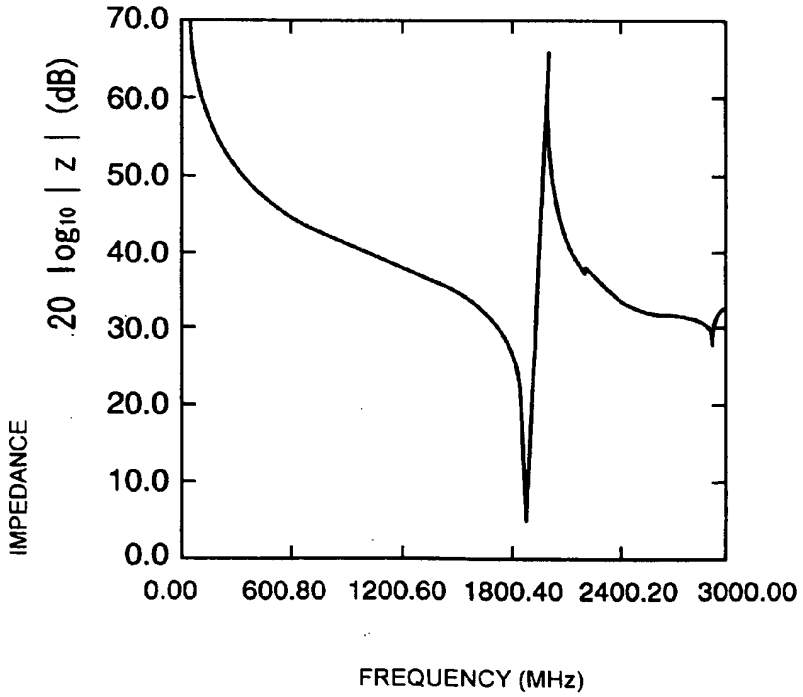
70.0
60.0
50.0
40.0
30.0
20.0
10.0
0.0
20 log10 | z | (dB)
IMPEDANCE
0.00
600.80
1200.60
1800.40
2400.20
3000.00
FREQUENCY (MHz)

FIG. 43

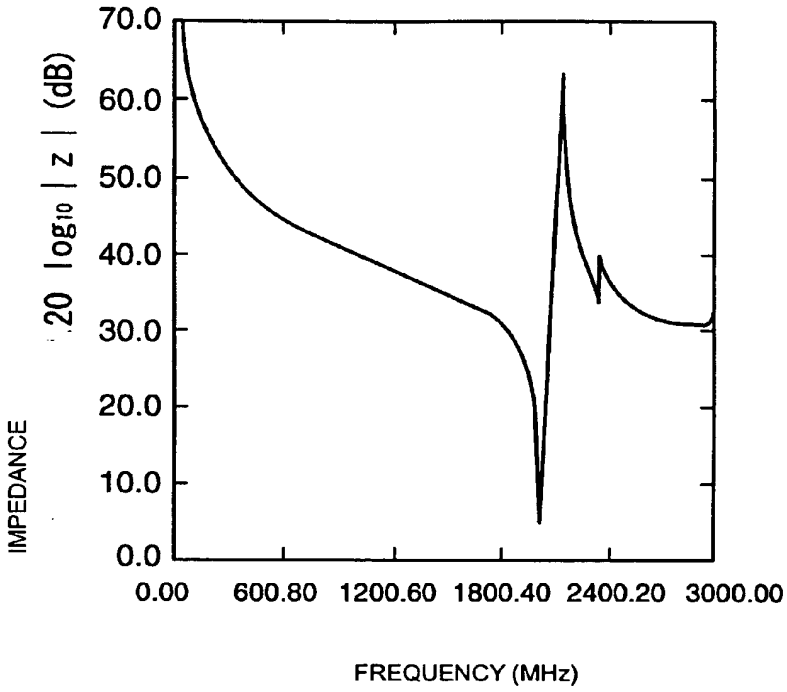
70.0
60.0
50.0
40.0
30.0
20.0
10.0
0.0
20 log10 | z | (dB)
IMPEDANCE
0.00
600.80
1200.60
1800.40
2400.20
3000.00
FREQUENCY (MHz)

FIG. 44

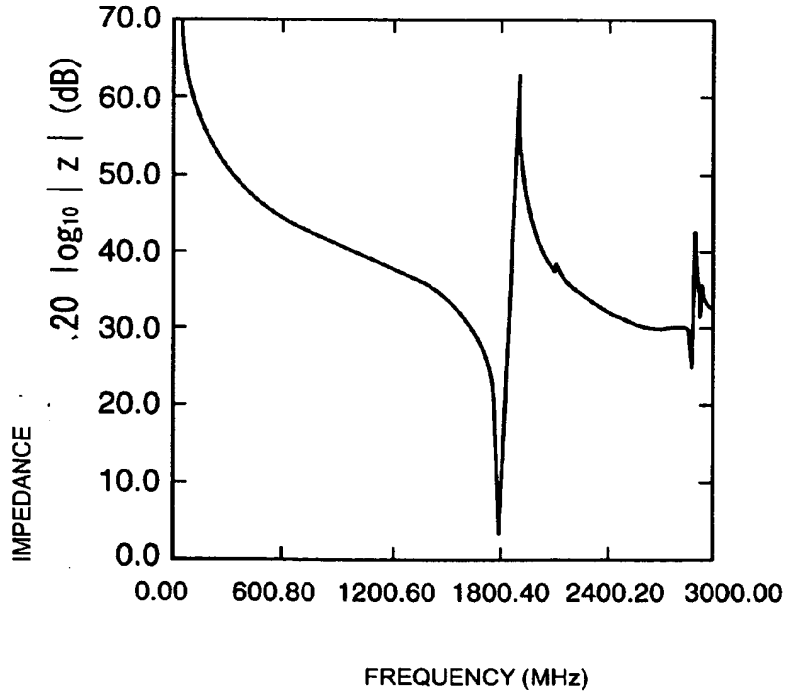
70.0
60.0
50.0
40.0
30.0
20.0
10.0
0.0
20 log10 | z | (dB)
IMPEDANCE
0.00
600.80
1200.60
1800.40
2400.20
3000.00
FREQUENCY (MHz)

FIG. 45

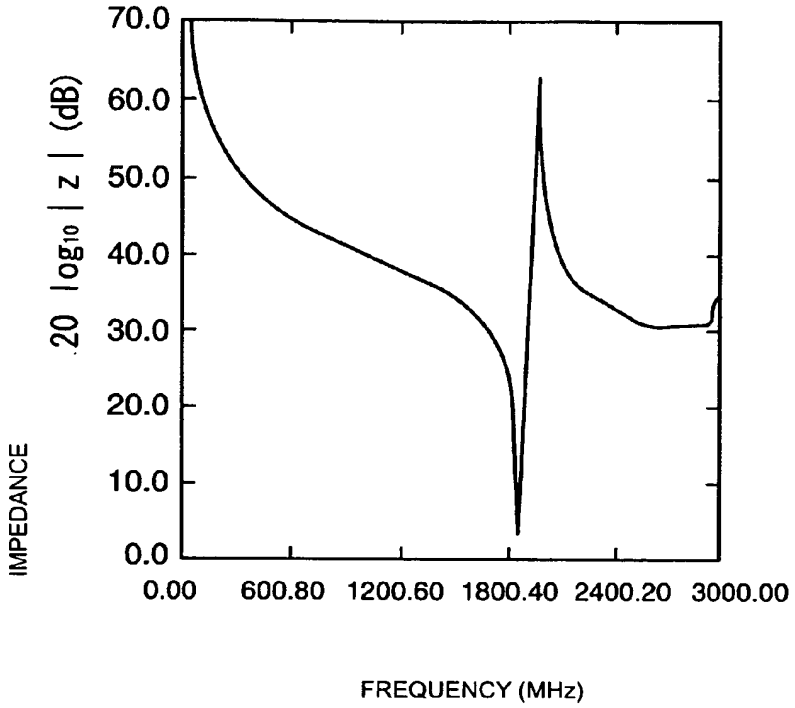
70.0
60.0
50.0
40.0
30.0
20.0
10.0
0.0
20 log10 | z | (dB)
IMPEDANCE
0.00
600.80
1200.60
1800.40
2400.20
3000.00
FREQUENCY (MHz)

FIG. 46

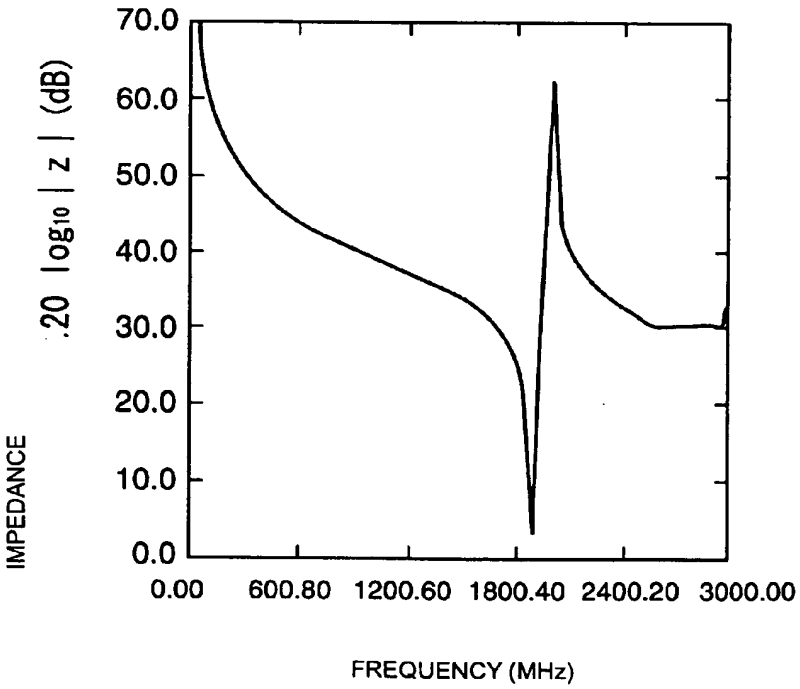
70.0
60.0
50.0
40.0
30.0
20.0
10.0
0.0
20 log10 | z | (dB)
IMPEDANCE
0.00
600.80
1200.60
1800.40
2400.20
3000.00
FREQUENCY (MHz)

FIG. 47

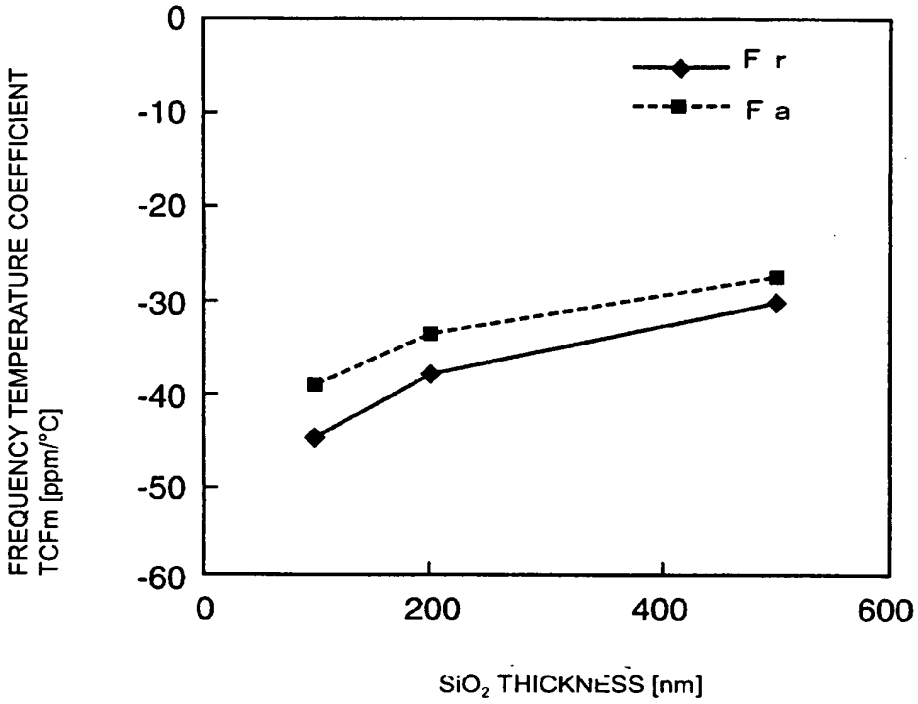
0
-10
-20
-30
-40
-50
-60
0
200
400
600
F r
F a
FREQUENCY TEMPERATURE COEFFICIENT
TCFm [ppm/°C]
SiO2 THICKNESS [nm]

FIG. 48

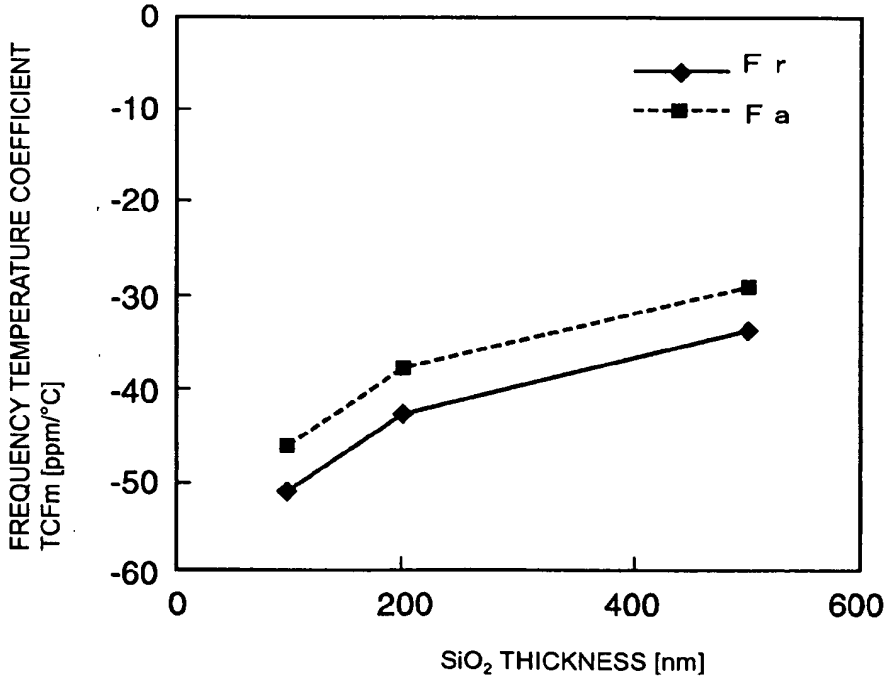
0
-10
-20
-30
-40
-50
-60
0
200
400
600
F r
F a
FREQUENCY TEMPERATURE COEFFICIENT
TCFm [ppm/°C]
SiO2 THICKNESS [nm]

FIG. 49

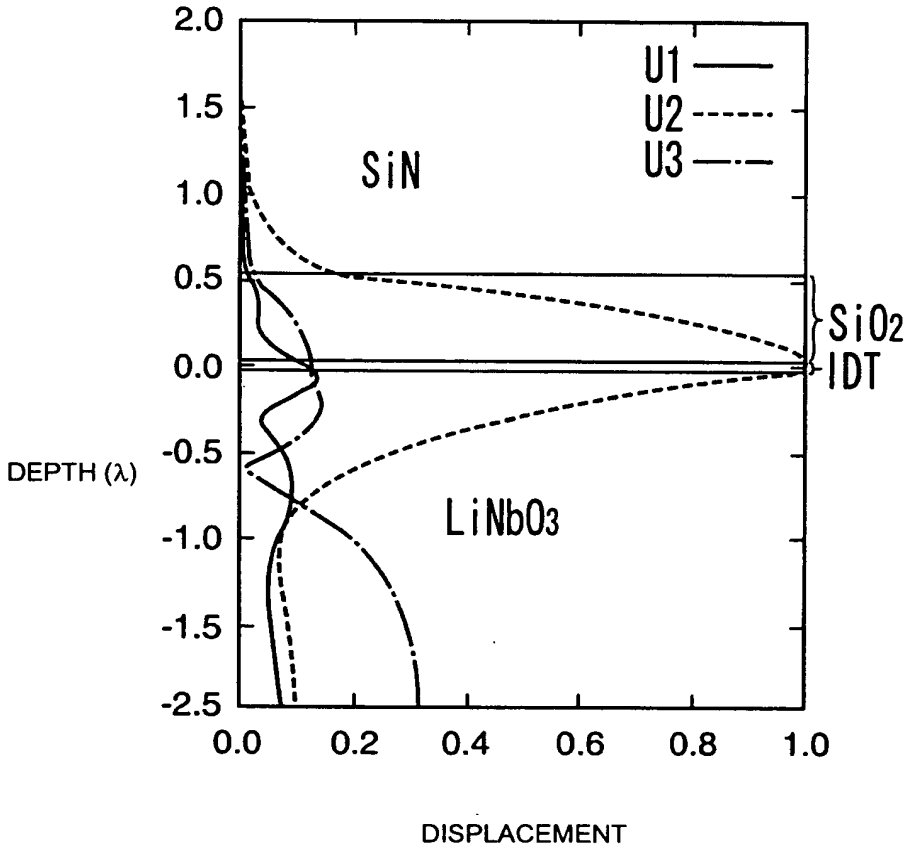
2.0
1.5
1.0
0.5
0.0
-0.5
-1.0
-1.5
-2.5
0.0
0.2
0.4
0.6
0.8
1.0
U1
U2
U3
SiN
SiO2
IDT
LiNbO3
DEPTH (λ)
DISPLACEMENT

FIG. 50

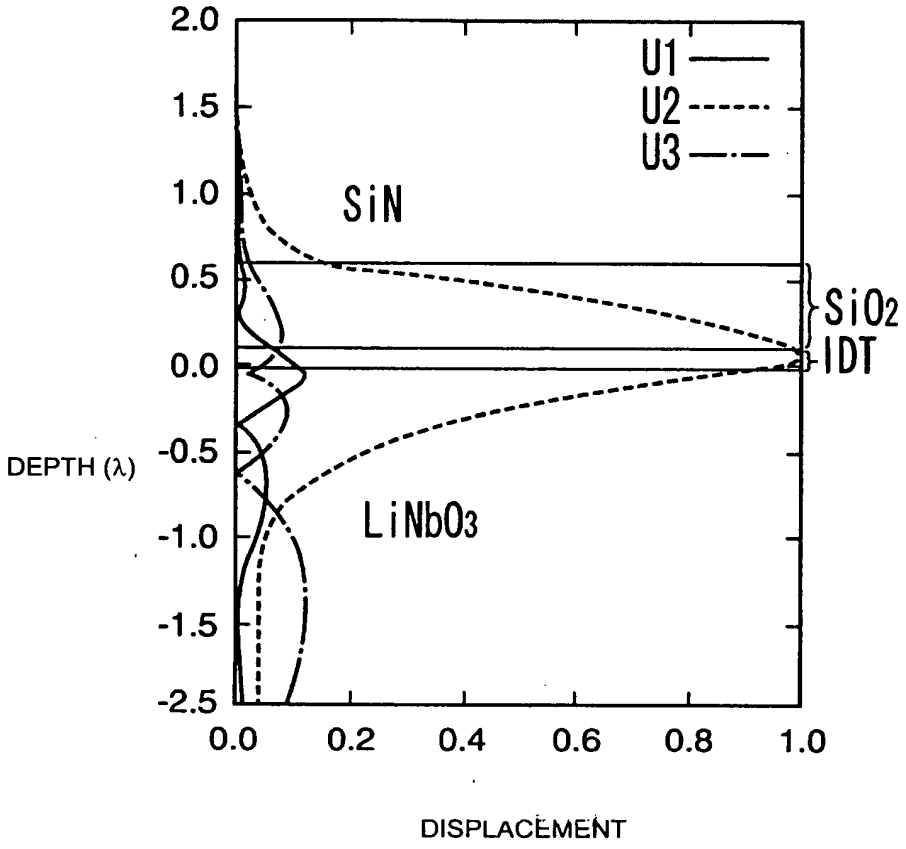
2.0
1.5
1.0
0.5
0.0
-0.5
-1.0
-1.5
-2.5
0.0
0.2
0.4
0.6
0.8
1.0
U1
U2
U3
SiN
SiO2
IDT
LiNbO3
DEPTH (λ)
DISPLACEMENT

FIG. 51

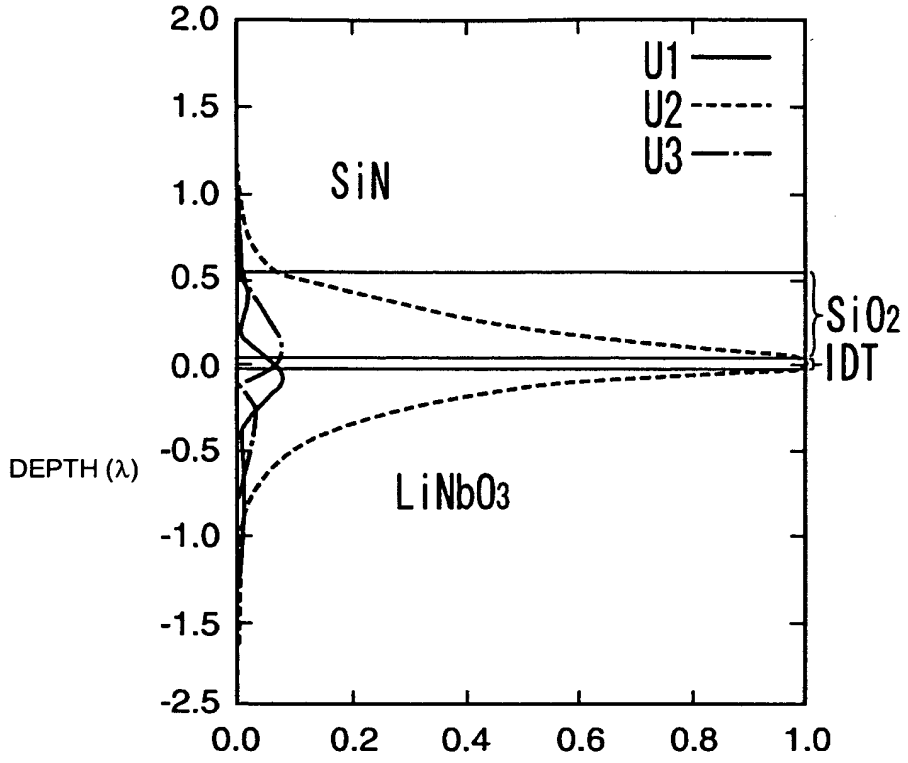
2.0
1.5
1.0
0.5
0.0
-0.5
-1.0
-1.5
-2.5
0.0
0.2
0.4
0.6
0.8
1.0
U1
U2
U3
SiN
SiO2
IDT
LiNbO3
DEPTH (λ)
DISPLACEMENT

INTERNATIONAL SEARCH REPORT

International application No.
PCT/JP2006/302693

A. CLASSIFICATION OF SUBJECT MATTER
H03H9/145(2006.01), ***H01L41/09***(2006.01), ***H01L41/18***(2006.01), ***H01L41/187***(2006.01), ***H03H9/25***(2006.01)

According to International Patent Classification (IPC) or to both national classification and IPC

B. FIELDS SEARCHED

Minimum documentation searched (classification system followed by classification symbols)
H03H3/08(2006.01), ***H03H3/10***(2006.01), ***H03H9/145***(2006.01), ***H03H9/25***(2006.01), ***H03H9/42***(2006.01), ***H03H9/44***(2006.01), ***H03H9/64***(2006.01), ***H03H9/68***(2006.01), ***H03H9/72***(2006.01), ***H03H9/76***(2006.01)

Documentation searched other than minimum documentation to the extent that such documents are included in the fields searched

Jitsuyo Shinan Koho	1922-1996	Jitsuyo Shinan Toroku Koho	1996-2006
Kokai Jitsuyo Shinan Koho	1971-2006	Toroku Jitsuyo Shinan Koho	1994-2006

Electronic data base consulted during the international search (name of data base and, where practicable, search terms used)

C. DOCUMENTS CONSIDERED TO BE RELEVANT

Category*	Citation of document, with indication, where appropriate, of the relevant passages	Relevant to claim No.
Y	WO 98/52279 A1 (Hitachi, Ltd.), 19 November, 1998 (19.11.98), Claims 13, 15; Figs. 5, 12; pages 9 to 13 (Family: none)	1-10
Y	WO 2004/070946 A1 (Murata Mfg. Co., Ltd.), 19 August, 2004 (19.08.04), Page 24 (example 1) to page 34 (example 3); Fig. 7 & EP 001610460 A1	1-10
Y	JP 2003-188679 A (Murata Mfg. Co., Ltd.), 04 July, 2003 (04.07.03), Par. No. [0045]; Fig. 14 & US 2003/0151329 A1	8-9

☒ Further documents are listed in the continuation of Box C. ☐ See patent family annex.

* Special categories of cited documents:
"A" document defining the general state of the art which is not considered to be of particular relevance
"E" earlier application or patent but published on or after the international filing date
"L" document which may throw doubts on priority claim(s) or which is cited to establish the publication date of another citation or other special reason (as specified)
"O" document referring to an oral disclosure, use, exhibition or other means
"P" document published prior to the international filing date but later than the priority date claimed
"T" later document published after the international filing date or priority date and not in conflict with the application but cited to understand the principle or theory underlying the invention
"X" document of particular relevance; the claimed invention cannot be considered novel or cannot be considered to involve an inventive step when the document is taken alone
"Y" document of particular relevance; the claimed invention cannot be considered to involve an inventive step when the document is combined with one or more other such documents, such combination being obvious to a person skilled in the art
"&" document member of the same patent family

Date of the actual completion of the international search 15 May, 2006 (15.05.06)	Date of mailing of the international search report 23 May, 2006 (23.05.06)
Name and mailing address of the ISA/ Japanese Patent Office Facsimile No.	Authorized officer Telephone No.

Form PCT/ISA/210 (second sheet) (April 2005)

INTERNATIONAL SEARCH REPORT

International application No.
PCT/JP2006/302693

C (Continuation). DOCUMENTS CONSIDERED TO BE RELEVANT

Category*	Citation of document, with indication, where appropriate, of the relevant passages	Relevant to claim No.
Y	JP 8-204493 A (Oki Electric Industry Co., Ltd.), 09 August, 1996 (09.08.96), Par. No. [0009]; Fig. 1 (Family: none)	8-9

Form PCT/ISA/210 (continuation of second sheet) (April 2005)

REFERENCES CITED IN THE DESCRIPTION

This list of references cited by the applicant is for the reader's convenience only. It does not form part of the European patent document. Even though great care has been taken in compiling the references, errors or omissions cannot be excluded and the EPO disclaims all liability in this regard.

Patent documents cited in the description

- WO 9852279 A **[0005]**

Non-patent literature cited in the description

- *IEICE material,* 1986, vol. S86-39, 47-4 **[0005]**
- *Nihon Onkyo Gakkai-shi,* 1980, vol. 36 (3), 140-145 **[0045]**
- **J. J. CAMPBELL ; W. R. JONES.** A method for estimating optimal cuts and propagation directions for excitation and propagation directions for excitation of piezoelectric surface waves. *IEEE Trans. Sonics and Ultrason.,* 1968, vol. SU-15, 209-217 **[0059]**

PUB-NO: EP001879291A1
DOCUMENT-IDENTIFIER: EP 1879291 A1
TITLE: BOUNDARY ACOUSTIC WAVE DEVICE
PUBN-DATE: January 16, 2008

INVENTOR-INFORMATION:

NAME	COUNTRY
KANDO, HAJIME	JP

ASSIGNEE-INFORMATION:

NAME	COUNTRY
MURATA MANUFACTURING CO	JP

APPL-NO: EP06713834
APPL-DATE: February 16, 2006

PRIORITY-DATA: JP2005126674A (April 25, 2005)

INT-CL (IPC): H03H009/02

EUR-CL (EPC): H03H009/02

ABSTRACT:

To provide a boundary acoustic wave device that efficiently confines the vibrational energy of boundary acoustic waves and exhibits a high electromechanical coupling coefficient, and is consequently not affected by higher-order modes. The boundary acoustic wave device includes a first

medium 11 having piezoelectric characteristics, a non-electroconductive second medium 12, and a third medium 13 through which slow transverse waves propagate at a lower acoustic velocity than slow transverse waves propagating through the first and second media 11 and 12. The first medium 11, the third medium 13, and the second medium 12 are stacked in that order. An IDT 14 is disposed between the first medium 11 and the third medium 13. The IDT 14 includes a metal layer made of a metal having a density Á in the range of 3000 to 21500 kg/m 3 . The IDT 14 has electrode fingers at a pitch of ? and has a thickness H1 satisfying the relationship 0.006? H1 0.2?, and the third medium 13 has a thickness H2 satisfying the relationship H1 < H2 0.7?.